TEXTURES AND MICROSTRUCTURES OF CONTROLLED ROLLED STEELS

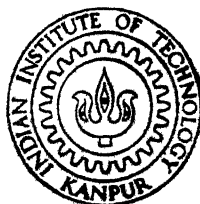*By*

ABHIRAM BHATTACHARJEE

DEPARTMENT OF METALLURGICAL ENGINEERING

INDIAN INSTITUTE OF TECHNOLOGY KANPUR

APRIL, 1991

TEXTURES AND MICROSTRUCTURES OF CONTROLLED ROLLED STEELS

A Thesis Submitted
in Partial Fulfilment of the Requirements
for the Degree of
MASTER OF TECHNOLOGY

By

ABHIRAM BHATTACHARJEE

to the

DEPARTMENT OF METALLURGICAL ENGINEERING
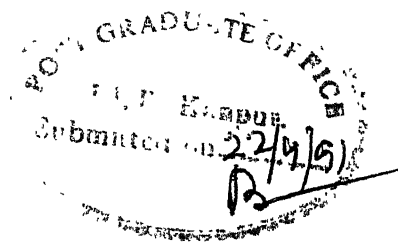
INDIAN INSTITUTE OF TECHNOLOGY KANPUR

APRIL, 1991

*Dedicated to
My Parents*

Certificate

Certified that the work reported in this thesis entitled 'Textures and Microstructures of Controlled Rolled Steels' by Mr. Abhiram Bhattacharjee has been carried out under my supervision and has not been submitted elsewhere for the award of a degree.

(R. K. RAY)
Professor

April, 1991   Department of Metallurgical Engineering
Indian Institute of Technology
Kanpur.

Certificate

Certified that the work reported in this thesis entitled 'Textures and Microstructures of Controlled Rolled Steels' by Mr. Abhiram Bhattacharjee has been carried out under my supervision and has not been submitted elsewhere for the award of a degree.

(R. K. RAY)
Professor

April, 1991   Department of Metallurgical Engineering
Indian Institute of Technology
Kanpur.

Acknowledgements

I take this opportunity to express my sincere gratitude and indebtedness to my supervisor, Prof. R.K. Ray for brilliant guidance and active co-operation throughout the course of this work.

I would like to thank M/s K.P. Mukherjee, H.C. Srivastava, S.C. Barthwal, R.P. Singh and B.K. Jain for assisting me at various stages of this work. Special thanks are due to Mr. B.K. Jain for tracing the figures and Mr. R.N. Srivastava for the excellent typing.

My acknowledgements are also due to Ms. Martha Patricia Butron-Guillen for drawing the pole-figures presented in this thesis.

- Abhiram Bhattacha

Contents

Synopsis

Studies have been carried out on a plain carbon and a microalloyed steel to find the effect of controlled rolling on crystallographic texture and microstructure, and to arrive at a useful correlation between the two. For this purpose a C-Mn steel and a Nb-V steel austenitized at two different temperatures of 1250°C and 1150°C, were subjectedto different controlled rolling schedule characterised by different amounts of deformation and finish rolling temperatures. Crystallographic textures of these were measured using the conventional pole-figure method. Structural characterisation of the samples were carried out using optical and transmission electron microscopy. Grain size measurement on all samples and grain size distribution measurement on a limited number of samples were also performed.

The ferrite grain sizes of the controlled rolled steels have been found to be dependent on the austenitizing temperature, amount of rolling reduction and finishing temperature. Finer ferrite grains are achieved for the Nb-V steel as compared to the plain C steel when other factors are kept constant. In general, controlled rolling at progressively lower temperatures, starting from γ recrystallization range and finishing in ferrite region produces the finest ferrite grain size. The structural details have been found to correlate well with the macroscopic textural results for both the steels. A sharp texture can be

related to either ferrite obtained from transformation of un-
recrystallized γ or ferrite which has been heavily deformed.
On the other hand a weak ferrite texture corresponds to nearly
equiaxed ferrite grains obtained predominantly by transforma-
tion from recrystallized γ.

Chapter I

Introduction

It has been known for many years that when structural steels are rolled to low finishing temperature, mechanical properties are improved [1]. The interpretation of this observation was given in terms of recrystallization after hot deformation with the ferrite grain size being reduced with decreasing deformation temperature in the austenite region [2].

In ship building and in other structural plates, after the World War II, the requirement of notch toughness was felt to counter the occurrence of brittle fracture. In some mills in Europe, practice of controlled low-temperature hot rolling was carried out, to increase notch toughness in hot rolled plate [3]. It was reported that though the strength increased largely, in as hot-rolled steel plates, by small addition of Nb, notch toughness deteriorated markedly. To prevent a reduction in notch toughness, the application of controlled rolling to Nb bearing steel was studied. This led to the establishment of the basis of combining controlled rolling with Nb steel.

The BISRA group in 1960s carried out research on controlled rolling which led the way in developing the present controlled rolling technology.

Controlled rolling has been developed for the major purpose of refining grain structure and thereby enhancing both the strength and toughness of steel in the as hot-rolled

condition. The fine ferrite grains are achieved by causing a refinement in the austenite structure. Controlling the rolling schedule to refine the austenite structure is the basic idea of the controlled rolling process.

Modern controlled rolling processes consist essentially of three stages: (a) deformation in the γ recrystallization region at high temperatures, (b) deformation in the γ non-recrystallization region within a low temperature range above Ar_3 and (c) deformation in the austenite-ferrite region. The reason for giving deformation in the γ non-recrystallization region is to divide an original austenite grain into several blocks by the introduction of deformation bands within it. Deformation in the austenite-ferrite region gives a mixed structure consisting of equiaxed grains and subgrains after transformation and, thus it further increases the strength and toughness.

The fundamental difference between conventionally hot-rolled and controlled rolled steels lies in the fact that nucleation of ferrite occurs exclusively at austenite grain boundaries in the former. But in the latter it occurs in the grain interior as well as at grain boundaries, leading to a more refined grain structure.

In controlled rolled steels, however, a crystallographic texture also develops during processing and this may cause planar anisotropies in mechanical properties.

Extensive work has been carried out regarding the effects of various deformation conditions on microstructure

and mechanical properties during controlled rolling. It has been found that a significant change in texture occurs along-with the changes in microstructure. The inheritance of a strong texture by the α phase from the γ during transformation depends principally on the severity of the rolling texture of the parent austenite. The intensity of the austenite rolling texture depends in turn on the amount of deformation to which the γ has been subjected, as well as on the temperature of deformation. Control of the processing variable to get desired properties by changing the microstructure suitably, often leads to an inadvertent modification of the crystallographic texture. This might result in a deviation from the desired final properties. Likewise, controlling the texture may also change the microstructure, thus changing the required properties. Since the textural and microstructural changes occur simultaneously and are interdependent, it has been reasoned that a correlation might exist between the two. No significant work is known to have been performed as yet in this direction.

The aim of the present investigation is to analyse the textural and microstructural results of a few controlled rolled steels and try to find a useful correlation between the two. For this purpose, a plain carbon and a microalloyed steel which have undergone different controlled rolling schedules were used. Optical metallography and transmission electron microscopy have been performed on the longitudinal

sections of the steel samples for structural characteriza-
tion. Crystallographic textures of these controlled rolled
samples were measured using the conventional pole figure
method. The results have been analysed and discussed suit-
ably.

Chapter II

Literature Review

2.1 Historical Development of Controlled Rolled Steels

Controlled rolling is a means of improving the proper-
ties of steel in the hot-rolled condition to a level equivalent
to, or greater than those of highly alloyed or heat-treated
steels. The development of controlled rolling started with the
basic idea of controlling process in order to refine the auste-
nite structure, and thereby to give fine ferrite grains.

In 1924 Arrowsmith [5] had pointed out the advantage
of grain refinement. Also, it was known that improvements in
mechanical properties result when steels are rolled to low
finishing temperatures [1]. The above idea was interpreted by
Hanemann and Lucke [2] in terms of recrystallization after hot
deformation with the α-grain size being reduced with decrea-
sing deformation temperature in the γ-region. Bari and Tipper
[6] in 1947 showed that in mild steel plates, the ductile-to-
brittle transition temperature was raised by an increase in
α-grain size. After examining as-rolled plates, Mackenzie [7]
showed a correlation between transition temperature and finish-
rolling temperature, a factor affecting γ-grain size. Other
investigators [8-13] have also reported similar results. All
these results have one factor in common: hot-rolling was
carried out as usual at high temperatures, and only the last

one or two passess were rolled at a lower temperature. Thus
these results were not always definite and were in disagree-
ment with each other.

In order to prevent the occurrence of brittle fracture,
notch toughness was required in shipbuilding and in other
structural steel plates. Instead of refinements of microstruc-
ture by Al killing and normalizing, controlled low-temperature
hot rolling was being practised by some mills in Europe to
provide increased notch toughness in hot-rolled plate [3].
The practice involved making the last few hot-rolling passess
at temperatures lower than normal.

Beiser [4] reported that small addition of Nb caused a
larger increase in strength but reduced notch toughness mar-
kedly in as-hot-rolled steel. In order to prevent a deterio-
ration in notch toughness, the application of controlled rolling
to Nb-bearing steel was studied. According to Noren's review
[14] (i) when hot-rolled under conventional rolling conditions,
Nb steel deteriorated markedly in toughness; (ii) when finish
rolled at lower temperatures, the improvement in toughness was
much greater for Nb steel than for Nb-free steel; and (iii)
when finish rolled below $800^{\circ}C$, or when total reduction below
$900^{\circ}C$ was more than 30% notch toughness improved remarkably.
On these methods, the basis of combining controlled rolling
with Nb steel was thus established.

Research on controlled rolling was carried out by the
BISRA group in 1960s, which opened the way for the development
of the present controlled rolling technology. Duckworth et al

[15] showed that with the C content below 0.1%, and by using Nb additions and a low finishing temperature with heavy draughting, very attractive properties could be obtained in the as-rolled condition. Philips and Chapman [16], Irani et al [17] and Jones and Rothwell [18] showed that Nb retarded recrystallization greatly, thereby enabling the deformation of γ in the non-recrystallization region, that transformation from deformed γ produced a fine α-grain structure, and that an improper draught schedule tended to cause a mixed grain structure.

Through further investigations, the importance of deformation in the non-recrystallization region was recognized. It was also made clear that controlled rolling was not to cease in the γ-region, but was to be extended into the γ-α region, thereby enhancing both strength and toughness. Modern controlled rolling means the overall technology consisting of (i) a suitable selection of chemical composition, (ii) a proper slab-reheating temperature to obtain small and uniform γ-grains, (iii) γ-grain refinement owing to repeated deformation recrystallization, (iv) deformation in the non-recrystallization region, (v) deformation in the γ-α two-phase region, and (vi) controlled cooling.

The Hall-Petch relation [10] correlates yield stress with ferrite grain size. Heslop and Petch [11] also associated transition temperature with grain size. They guided the development of controlled rolling throughout its whole course.

The processes that give rise to textures and texture changes in wrought steels are of three types, namely, deformation,

recrystallization, and transformation. For the production of
sheet materials, where most of the processing is carried out
in the ferrite phase, texture control is achieved largely by
controlling the first two processes i.e. deformation and annea-
ling, or recrystallization. Here, the γ-to -α transformation
only plays a minor role by providing the starting texture for
the cold rolling operation. The effects of rolling reduction,
heating rate, holding temperature, and alloying on the annea-
ling textures formed in low carbon and deep drawing steels
have been reviewed by Mishra and Darmann [19] and by Hutchinson
[20]. A review by Tanaka [21] covers several aspects of the
controlled rolling process, including ferrite grain refine-
ment, the properties of controlled rolled steels and industrial
controlled rolling practices. But, it does not deal with the
effect of transformation on the textures found in hot and
controlled rolled steels. The properties of such materials
are dictated, not only by the ferrite grain size and presence
of solute elements and precipitates, but also by the overall
crystallographic texture of the grains.

The various kinds of transformation textures encoun-
tered in steels and their possible modes of origin have been
briefly surveyed by Inagaki [22] in 1981. Inagaki and Kodama
studied the development of texture in several Nb and Nb-V
steels, finished at various temperatures. In 1990, Ray and
Jonas [23] carried out an up to date review of several aspects
of transformation textures, especially in controlled rolled
steels.

2.2 Different Controlled Rolling Schedules

Refinement of the ferrite structure is achieved mainly through austenite grain refinement because of the relation between austenite and ferrite grain sizes. The change in grain structure with deformation temperature has been studied by many investigators. Many studies were confined to deformation in the γ-region alone while few of them were extended to deformation in the γ-α two phase region.

Kozasu et al [24] divided deformation temperatures in the γ-region into three ranges in association with the change in austenite and ferrite grain structures. Deformation above $1000^{O}C$ brings about coarse, recrystallized austenite grains, which transform to a relatively coarse ferrite and upper bainitic structure (range 1). Deformation in the intermediate temperature range from $1000^{O}C$ to $900^{O}C$ refines austenite by repeated recrystallization, leading to fine-grained ferrite (range 2). Deformation below the recrystallization temperature produces 'warm-worked' austenite, which leads to a finer α-grain structure (range 3). The grain refinement is achieved mainly by deformation in ranges 2 and 3 [25]. The transition temperature was shown to decrease in a linear manner with an increase in total reduction in ranges 2 and 3 [25].

From a practical viewpoint, Baird and Preston [26] proposed a similar but slightly different interpretation. Figure 2.1 depicts the rolling procedures involving reduction in the rapid-recrystallization region (range 1), delay in rolling (in range 2) and final reduction in the non-recrystal-

lization region (range 3). To ensure the required amount of deformation in the non-recrystallization region, the delay in rolling was necessary. During the delay, however, partial recrystallization tends to occur which leads to the formation of a mixed grain structure.

According to Fukuda et al [27, 28] during hot-rolling there are two types of austenite to ferrite transformation mode shown in Figure 2.2. Type 1 is the transformation from recrystallized γ to α, where α nucleation takes place exclusively at recrystallized γ-grain boundaries. Type 1 is subdivided into two, A and B: Type 1A and 1B are equivalent to range 1 and 2 above, respectively. Rolling passes at high temperatures do not contribute to the refinement of the γ-grain structure (γ-grain size $\lesssim$ ASTM 5), which transforms to a coarse α and/or Widmanstatten-like structure (type 1A). Deformation at low temperatures in the recrystallization region produces a fine-grained γ-structure (γ-grain size $\gtrsim$ ASTM 6), which transforms to a fine-grained ferrite-pearlite structure (type 1B). Type 2 is the transformation mode from unrecrystallized γ to α, where α nucleation occurs at grain interiors as well as grain boundaries and fine α-grains are obtained. The transition type is in the intermediate mode between types 1 and 2, giving a mixed grain structure. When compared it is found that the finest α-grain is obtained by type 2, followed by type 1B, transition type, and type 1A. However, α-grain structure is more homogeneous for type 1B than for type 2.

Sekine and Maruyama [29] showed that α-grain structure is decided by the recrystallized γ-grain size before deformation in the non-recrystallization region and the amount of deformation in that region. Figure 2.3 depicts the effect of total reduction in the non-recrystallization region on α-grain size and upper bainite volume fraction. When a recrystallized γ-grain size is large, it is difficult to suppress the formation of upper bainite even by large deformation. However, when the recrystallized grain size is small, upper bainite is not allowed to form, even with moderate deformation, giving fine grained α. They emphasized that the best way is to refine γ through recrystallization as much as possible (type 1B), followed by deformation in the non-recrystallization region (type 2) and whereby a uniform, fine-grained α-structure is produced.

The difference between Fukuda et al [27] and Sekine and Maruyama [29] is that the former stressed type 2 to achieve a fine-grained α-structure, whereas the latter emphasized the importance of the combination of types 1B and 2. According to Tanaka [21] this argument is reduced to the uniformity of α nucleation with unrecrystallized γ-grains which, in turn, is reduced to the uniformity in deformation-band density throughout unrecrystallized grains, since α nucleates on deformation bands as well as at γ-grain boundaries. There has been some evidence that deformation-band density tends to be heterogeneous and that not all the deformation bands have the same ferrite-nucleating potential [30, 29] suggesting that type 2

tends to produce a mixed α-grain structure compared with the optimum combination of types 1B and 2.

Coleman et al [31] and Gladman and Dulieu [32] obtained a further increase in strength by extending deformation into the γ + α and/or α-regions, and by developing a substructure. Advancing this idea Tanaka et al [33, 34] proposed the three stages of the controlled rolling process. Figure 2.4 illustrates schematically the three stages of the controlled rolling process, and the microstructural change accompanying deformation in each stage.

Stage 1: Coarse austenite a is refined by repeated deformation and recrystallization b, but still transforms to relatively coarse ferrite b'.

Stage 2: Deformation bands are formed in elongated, unrecrystallized austenite c, and ferrite nucleates on the deformation bands as well as γ-grain boundaries, giving fine α c'.

Stage 3: Deformation in the γ - α two-phase region continues stage 2 and also deforms the ferrite, producing a substructure d.

During cooling after deformation, unrecrystallized austenite transforms to equiaxed α-grains, while deformed ferrite changes into subgrains d'.

Grain refinement through repeated recrystallization does not proceed indefinitely but reaches a certain limiting value b and thereby results in relatively coarse α-grains b'. To break the limiting value we can divide the γ-grain. Since

a recrystallized γ-grain b is divided by deformation bands c,
the final α-grain structure is much smaller for c' than for b'.
The deformation in the two-phase region causes further grain
refinement and a mixed structure consisting of equiaxed grains
and subgrains. Since unrecrystallized γ containing deforma-
tion bands promotes the γ to α transformation, from a different
viewpoint, controlled rolling can be defined as a process for
accelerating α transformation and thereby for producing fine-
grained α in steel with medium hardenability which, without
being controlled rolled, will transform to a bainitic struc-
ture, giving poor toughness.

2.3 Controlled Rolling and Microstructure

2.3.1 Deformation in the γ Recrystallization Region

2.3.1.1 Dynamic Recrystallization

The two kinds of restoration processes associated
with hot working are dynamic and static recrystallization [35].
At high temperatures when steel is deformed in the austenitic
state, the flow stress rises to a maximum and then falls to a
steady state. In a range of strain less than that for the
peak stress dynamic recovery operates, while in the steady-
state region dynamic recrystallization occurs. This is shown
in Figure 2.5. The structures developed by dynamic restora-
tion are thermodynamically unstable, and when held at the
temperature they are modified by the static restoration process.

The dynamically recrystallized grain size d is asso-
ciated with the Zener-Hollomon parameter Z, which is a

temperature-compensated strain rate, and is given by the following equations

$$d^{-1} \propto \sigma_{flow} \propto \log Z$$

$$Z = \dot{\varepsilon} \exp(Q_{dif.}/RT)$$

where

$\dot{\varepsilon}$: strain rate

$Q_{dif.}$: activation energy for self-diffusion of iron

R : gas constant

T : absolute temperature.

However, since a critical strain for the onset of steady state is very large, even at high temperatures [35, 36] it is almost impossible to hot roll steel, and in particular Nb steel, in the steady-state region. Therefore, it is almost impossible to refine the γ-grain through dynamic recrystallization. Instead, grain refinement must be achieved by static recrystallization.

2.3.1.2 Static Recrystallization

In static recrystallization after hot deformation, nucleation sites for new grains are predominantly triple junctions of grains and grain boundaries, and nucleation within grains is almost nil [24]. The distribution of nuclei is highly localized and inhomogeneous. Some grain boundaries give rise to numerous nuclei while there are others where nuclei are completely absent [24]. The progress of recrystallization after nucleation is essentially the migration of the

recrystallizing front into the deformed matrix as is usual in recrystallization. The completion of recrystallization is followed by normal grain growth.

Effects of the amount of deformation and deformation temperature on recrystallized grain size are shown in Figure 2.6. The recrystallized grain size decreases rapidly as the amount of reduction increases, reaching a limiting value [33]. The limiting grain size decreases with reducing initial grain size [37]. Although a lower deformation temperature produces smaller grain sizes, the effect of temperature is slight.

Since nucleation sites for recrystallization are pre-dominantly at the grain boundaries [24], the initial grain size plays an important role in determining recrystallized grain size. Using stainless steel, Towle and Gladman [38] showed that recrystallized grain size d_{rex} can be expressed by:

$$d_{rex} = k \ \varepsilon^{-0.5} \ d_o \ Z^{-0.06}$$

where k is a constant, ε is the amount of strain, d_o is the initial grain size and Z is the Zener-Hollomon parameter. This equation also indicates the slight effect of strain rate on recrystallized grain size.

2.3.1.3 Conditions for Recrystallization

Static recrystallization accompanying hot deformation does not occur under all conditions. It is necessary to apply more deformation than that required for recrystallization. As is the temperature dependence in plain C steel, the critical

amount of deformation, R_{crit}, required for the completion of recrystallization is also small. However, in Nb steel, R_{crit} is very large and its temperature dependence is substantially higher [33].

Ouchi et al [39] and Tanaka et al [40, 41, 42] studied the general recrystallization behaviour by single-pass rolling. This is shown in Figure 2.7. The recrystallization behaviour is divided into three regions: recovery, partial recrystallization, and recrystallization. The recrystallization region is subdivided into two regions - the static region and the dynamic region.

As seen from Figure 2.7, it is very difficult to roll steel in the recrystallization region during the initial passes in the plate mill since R_{crit} is extremely large. In practice, rolling passess are carried out in the recovery region or, at most, in the partial recrystallization region. If the initial rolling passes are made in the recovery region, huge grains are formed locally owing to the strain induced grain boundary migration which persists through the whole course of rolling. These large grains transform to upper bainite and/or coarse ferrite grains, giving poor toughness. On the other hand, if a reduction per pass greater than that for partial recrystallization is given successively, a uniform and refined grain structure is obtained.

It is considered that the strain-induced precipitation of fine $Nb(C,N)$ is the reason that the critical amount of

reduction required for recrystallization and its temperature dependence is much larger for Nb steel than for plain C steel [39, 43].

2.3.1.4 Formation of Mixed Grain Structure

A finer α-grain size is produced in case of controlled rolling than in case of conventional hot rolling and normalizing. But controlled rolled steel often exhibits a mixed structure consisting of fine and coarse α-grains and/or upper bainite, decreasing low-temperature toughness.

The mixed grain structure of the α grains is due to that of the γ grains. When partial recrystallization occurs, fine recrystallized grains are formed at the γ-grain boundaries and hence an unrecrystallized region is left in the grain interior where the mixed γ-grain structure is produced [18]. If coarse γ grains are formed or when rapid grain growth takes place after recrystallization owing to unsuitable deformation conditions, a mixed γ-grain structure tends to be formed [44]. Once a mixed γ-grain structure is formed, it cannot be eliminated by later rolling passes . This is because when rolled again, the recrystallized region near the grain boundaries in the earlier pass recrystallizes preferentially as the grain size in this part is much smaller than the unrecrystallized region at the grain interior. A 'continuous' schedule involving reduction in the whole temperature range [18] or suitable conditions of holding [17, 44] are ways of preventing a mixed grain structure.

2.3.2 Deformation in the γ Non-Recrystallization Region

2.3.2.1 Retardation of Recrystallization

Following deformation in the recrystallization region, deformation in the non-recrystallization must be applied in order to decrease the grain size further.

In plain C steels, recrystallization becomes sluggish at low temperatures in the γ-region (i.e. about $900^{\circ}C \simeq Ar_3$) [45, 46]. Nb can powerfully influence the retardation of γ-recrystallization, thereby achieving a non-recrystallized state. While Al and Al + N accelerates recrystallization slightly, V has some retarding effect while Nb has a very large retarding effect. This was reported by Kozasu et al [24]. The stronger retarding effect of Nb is due to the differences in solubility of Nb and V in γ and strain-induced precipitation potential between the two elements. The retardation of recrystallization due to Nb can be exhibited only when Nb is in solution in γ before deformation.

The retardation of recrystallization due to Nb has been attributed to the following causes: (i) a solute drag effect [47-51], (ii) strain-induced precipitation of fine Nb (C,N) [17, 18, 52-60], or (iii) the combined effects of solute Nb and precipitation of fine Nb(C,N) [48-51]. It was reported by Coladas et al [50] that the main influence of Nb as an alloying element was on the incubation time required for the start of recrystallization and not on the recrystallization

kinetics after incubation. He also reported that the delayed recrystallization is due to solute drag effect.

2.3.2.2 Formation of Deformation Band

Usually, the α-grains are found to nucleate in deformation bands as well as the γ-grain boundaries. Though the nature of deformation bands is not exactly known, they are generally found to exist in closely packed pairs of parallel lines which often terminate within a grain, creating a twin-like pattern in heterogeneous distribution. Sekine and Maruyama [29] said that the apparent γ-grain boundary area (γ-grain boundary and the deformation bands together) increases with an increasing amount of reduction. A steady level is reached above ~30% reduction. When the amount of reduction increases, the γ-grain-boundary area increases gradually while the deformation-band density increases rapidly. This indicates that the α-grain refinement resulting from deformation in the non-recrystallization region is mainly due to an increase in the deformation band. Even when the deformation band is saturated in number, about 10% of the γ-grains contain very few deformation bands [29]. All deformation bands do not have the same ferrite-nucleation potential [30]. Decrease in recrystallized γ-grain size before deformation in the non-recrystallization region can lead to a reduction of inhomogeneity in grain structure.

When about 70-80% reduction is given to finely recrystallized γ grains in practice, in the non-recrystallization

region, the ASTM grain-size number is ~12. But normalization
produces, at most, a grain size number of ~10.

2.3.3 Deformation in Austenite-Ferrite Region

A limiting γ-grain size which was achieved by deform-
ation in the recrystallization region is broken by deformation
in the non-recrystallization region. The limiting value is
reached at about 60-70% reduction in the non-recrystallization
region. This limit can only be broken by deformation in the
γ - α two phase region. In the twophase region, deformation
produces a mixed grain structure which consists of polygonal
grains and subgrains. Polygonal α are formed from the deformed
γ by transformation, while the deformed α changes into sub-
grains. In deformed α, the recrystallization process is very
sluggish and subgrains are produced. This happens due to the
stabilization of the α sub-boundary network by strain-induced
precipitation of $Nb(C,N)$ and/or $V(C,N)$ [18, 47, 52, 58, 61].
The α grains formed impinge on the pre-existing γ-subgrains and
hence cannot grow further. This sort of a mutual interaction
between deformed γ and α produces a further decrease in α-
grain size.

A duplex structure consisting of soft polygonal grains
and hard subgrains is produced by deformation in the two-phase
region. But deformation of γ produces a single structure con-
sisting of soft grains alone. Hence a difference in mechanical
properties is brought about by this difference in microstruc-
ture between the two controlled rolling conditions.

2.4   Representation of Texture

Texture or preferred orientation with respect to some crystallographic planes and directions exists to some extent in controlled rolled steels. The microstructure and mechanical properties in addition to others are affected by this texture. The usual representation of textures are by pole figures which are simple stereographic projections showing distribution of particular crystallographic directions in a group of grains constituting the metal. The reference directions in pole-figures are taken as some well-defined directions. The rolling direction (RD), transverse direction (TD) and normal direction (ND) are the three reference directions in case of rolled materials. The procedure for representing texture by pole-figures is illustrated in Figures 2.8(a) to (e). The sheet is made to sit at the centre of the stereographic sphere and the RD, TD and ND coincide with the X, Y and Z axes (Figure 2.8a). The orientation of a grain, say (100), can be then represented easily by plotting the three (100) poles in a pole-figure. All the poles concerned are normally projected on to the equitorial plane producing a stereographic projection (Figure 2.8b). When the poles are uniformly distributed over the area of projection then no texture is said to exist and the specimen is said to possess a 'random' texture. If the poles tend to cluster together in certain areas of the pole-figure, they are said to produce a texture (Figure 2.8c). Usually, the data is collected from many grains simultaneously and are represented in the form of density contours on the pole-figure (Figure 2.8d-e).

In texture work X-ray diffraction is used to measure pole-figures. Two methods, the transmission method due to Decker, Asp and Harker [62] and back reflection method by Schulz [63] are available. Quantitative measurements are not possible from pole-figures as they specify only two independent variables while there are three degrees of freedom in the general orientation. The pole figures are thus only projections of the three-dimensional orientation distribution function (O.D.F.) which describes the orientation density in a three-dimensional orientation space formed by the Euler angles $\emptyset_1$, $\emptyset$ and $\emptyset_2$, giving the rotation of the crystallographic axes into the specimen co-ordinate system. Figure 2.9 shows the transformation of the sample frame S to the crystallite frame using Euler angles, by the following three steps:

(i)   A first rotation $\emptyset_1$ around the ND transforms the TD and the RD into the new directions TD' and RD' respectively. $\emptyset_1$ must have such a value that RD' is perpendicular to the frame formed by ND and [001].

(ii)   A second rotation $\emptyset$ around the new direction RD' has such a value that it transforms ND into [001] (= ND') and TD' into TD".

(iii)   A third rotation $\emptyset_2$ around [001] (= ND') transforms RD' into [100] and TD" into [010].

The O.D.F. is then mostly plotted by contour lines in a series of sections through the Euler space. The selected area diffraction method of measuring O.D.F. by the transmission electron microscope using thin foils being very laborious,

O.D.F.'s are reproduced nowadays from a series of pole figures by the application of the series expansion method. In this method the O.D.F. is expanded in a series of generalised spherical harmonics $C_\lambda^{mn} T_\lambda^{mn}$ ($\emptyset_1 \emptyset \emptyset_2$) and the expansion co-efficients C_λ^{mn} are derived from the corresponding series expansion of the pole-density distributions (pole-figures).

2.5 Controlled Rolling and Crystallographic Texture

In controlled rolling of steels reductions are applied in the recrystallized and unrecrystallized γ region, followed by deformation in the intercritical ($\alpha + \gamma$) region before controlled cooling to room temperature. The properties of such materials are dictated, not only by the ferrite grain size and presence of solute elements and precipitates, but also by the overall crystallographic texture of the grains. The three types of processes that give rise to textures and their changes are deformation, recrystallization and transformation. In this case the texture changes accompanying transformation play a much larger role.

Depending on the type and amount of alloying elements in a given steel, the cooling rate after deformation processing, and the 'state' of the austenite (i.e. strain free or worked), the austenite can transform:

(a) by a diffusional mode to polygonal ferrite or pearlite.

(b) by a shear mode to martensite.

(c) by mixed diffusion and shear modes to acicular ferrite or bainite.

If the parent material (austenite) possesses a crystallographic

texture, the material after transformation (ferrite, martensite, acicular ferrite or bainite) will also acquire a texture that can be related in a precise way to the parent material texture. Thus, textures present in the high temperature γ phase can be inherited by the transformation products.

There are various orientation relationships proposed by many investigators relating the crystallographic orientations in parent and product structures. Three main orientation relationships between γ and α in steels are given in Table 2.1. Experimental evidence indicates that the K-S orientation relationship is generally followed during the austenite-ferrite or martensite transformation in steels [64, 65] when strong textures are produced in rolled γ, the texture inherited by the transformed α is invariably much weaker due to the multiplicity of the transformation variants.

2.5.1 Textures in Deformed and Recrystallized Austenite

In the upper temperature ranges of hot working static recrystallization takes place. At lower temperatures of hot-working rolling is followed by either static recrystallisation (in plain C and similar steels) or by the absence of recrystallization and pan-caking (in Nb steels). Pan-caking occurs when the time available for carbonitride precipitation is sufficient to prevent static recrystallization. In presence of Nb rapid static recrystallization is prevented. In this case when time is short dynamic recrystallization followed by post-dynamic recrystallization takes place [66]. All three of

these processes (i.e. deformation, precipitation and recryst-
allization) give rise to the development of microstructural
directionalities. When the austenite recrystallizes before
transformation, only a weak transformed texture is present in
ferrite [22]. Much sharper textures are produced in controlled
rolled steels which are finished below the non-recrystallization
temperature.

From the results of a number of studies [67] it is now
clear that the general features of the austenite rolling tex-
ture normally consists of orientations running from {110} <112>
to near {4 4 11} <11 11 8>. Major component of the austenite
recrystallization texture is the cube, {100} <001>.

2.5.2 Effect of the Different Stages of Controlled Rolling on Transformation Texture

The strength of the texture inherited by α from the γ
during transformation depends on the severity of the rolling
texture of the parent austenite. The greater the amount of
reduction at a particular temperature, the more severe will be
the γ rolling texture. The γ rolling texture is also affected
by the temperature of deformation which has been explained in
the last section. The influence of the rolling parameters in
the stages of controlled rolling on the resulting transforma-
tion texture is given below.

2.5.2.1 Deformation in Recrystallized γ Region

In this stage grain refinement takes place through
static recrystallization [35]. This phenomenon proceeds in a

manner similar to that in cold worked materials, and is foll-
owed by normal grain growth. The critical amount of deforma-
tion needed for the completion of recrystallisation during hot
working $\varepsilon_{crit.}$, is larger than at room temperature and its
temperature dependence is higher in Nb than in plain C steels
[33]. This difference can be attributed to the formation of
strain induced Nb(C,N) precipitates in the Nb steels [39, 43]
so that static recrystallization is essentially suppressed
during rolling below 950°C [21].

The hot rolling of low-C steels at temperatures above
the austenite recrystallization temperature generally produces
a rather weak transformation texture [22]. Kallend et al [68]
determined the O.D.F. of the ferrite in a 0.11 C-0.35 Si-1.35
Mn-0.052 Nb steel finished at a temperature of 1000°C after
80% reduction by rolling. The ferrite texture was rather weak
and consists mostly of the {100} <011> component which origi-
nates from the cube {100} <001> component of the austenite
recrystallization texture.

2.5.2.2 Deformation in Unrecrystallized γ Region

This stage introduces a high density of deformation
bands into the matrix. The ferrite nucleation takes place at
both grain boundaries and grain interiors leading to a finer
grain size. The strong deformation textures produced by heavy
amounts of deformation can be retained in the austenite in this
stage due to effective retardation of recrystallization.

Using O.D.F. analysis, Inagaki [69] showed that, for
a Nb-V steel, texture of specimens finished at 850°C consists

of two major components namely the {332} <113> and {113} ∼

{4 4 11} <110>. These originate, respectively, from {110} <112>

and {112} <111> which are the rolling texture components of the

parent austenite. Many previous investigations [22, 68, 70,

71, 72, 73, 74] have also shown similar results in the trans-

formation product texture. When the finishing temperature is

decreased within this range, there is an increase in the seve-

rity of the transformation texture. This is explained in terms

of an increase in the sharpness of the original austenite

rolling texture.

The textures of specimens of simple C-Mn steel are

seen to be considerably weaker than those of the Nb-V steel

finished at the same temperature [69]. The main texture compo-

nents here can be broadly identified as {554} <225> (near

{332} <113>) and {100} <011>. The former component appears as

broader and of much lower intensity in the Nb-V free steel than

in Nb-V steel. This can be attributed to the greater accumu-

lated strain in the non-recrystallization regions in the

microalloyed as opposed to the plain C steel. The {100} <011>

component arises as a result of α texture inherited from the

cube texture formed in the partly recrystallized austenite in

Nb-V free steel.

2.5.2.3 Deformation in (γ + α) Region

During controlled rolling, the deformation of steel

in (γ + α) region has been found to produce finer α grain

sizes [21]. In addition, improvement in yield and ultimate

tensile strengths are also achieved [33, 31, 75]. During such rolling, the processes which take place in steel are (i) crystal rotation of the parent γ phase, (ii) $\gamma \to \alpha$ phase transformation, and (iii) crystal rotation and possible recrystallization of the product α phase. The resultant texture of the steel is therefore quite complex and largely influenced by the relative contributions of these three processes which, in turn, depend on the composition, temperature, amount of reduction in each pan, and the finishing temperature. The final texture is made up of the accumulated components of the $\gamma \to \alpha$ transformation texture and the hot rolling texture component of the α phase. When the finishing temperature lies in the upper $(\gamma + \alpha)$ range, the amount of α phase formed, before the final pass, is relatively small. In such a case, the contribution of crystal rotation in the α phase to the overall texture is not too significant. On the other hand, when finishing temperature lies in the lower $(\gamma + \alpha)$ range, most of the γ phase has already changed to α before the final passes. The α grains formed earlier at higher temperatures, which inherit the γ rolling texture, experience further deformation at lower temperatures, which further sharpens the texture of the ferrite phase. The remaining γ are also deformed continuously resulting in an increase in the γ texture and is eventually inherited by the transformed α phase.

Investigations [76] have shown that in a Nb-steel increasing the amount of deformation in the $(\gamma + \alpha)$ region led to an increase in the severity of the original texture of the

material. Inagaki and Kodama [69, 77] studied the development of texture in several Nb and Nb-V steels finished at various temperatures. They found that, for specimens finished at just above the Ar_3 temperature, the main orientations of the α texture were {332} <113> and {113} ∽ {112} <110>. These get progressively modified as a result of deformation of the α phase when the finishing temperature is lowered. The changes that have been identified are (i) {332} <113> ⇀ {554} <225> → {111} <112> and (ii) {113} <110> ⇀ {112} <110> → {223} <110>. The orientations listed in (i) have a common <110> direction parallel to TD, whereas the orientations in (ii) have a common <110> direction parallel to RD. Theoretical calculations [78] show that the end texture of {111} <112> in (i) can be obtained whereas the {112} <110> intermediate component in (ii) is too stable to undergo further reorientation. Thus the {113} <110> component of the transformation texture is not converted to components of the γ fibre ({111} ⊥ ND), which are the ones required for good deep drawability in steels. They also show that {111} <112> in (i) above is gradually converted by rolling to {111} <110> component. Both are important components of γ fibre.

Some plots of R versus the angle α with respect to the rolling direction are given in Figure 2.10. It is clear from these that for high $\bar{R}$ values i.e. good deep drawability the {332} <113>, {554} <225>, {111} <112> and {111} <110> texture components are preferred over all the others. Thus the presence of {332} <113> as the main starting component is

desirable before processing in $(\gamma + \alpha)$ and α ranges. Inagaki et al [79] attempted to establish a quantitative relationship between the transformation textures of controlled rolled steels and their mechanical anisotropies. Anisotropies in relative yield stress and of the orientation factor for brittle fracture, $\cos^2\theta$, which is a measure of the toughness were calculated for various ideal orientations [79]. Figures 2.11 and 2.12 show that {113} <110> component in the transformation texture is undesirable due to significant anisotropy in both and its tendency to make the material brittle along planes oriented at 45° with respect to the rolling direction. {332} <113> component leads to much better strength and toughness properties.

Thus, we can see that the strength, toughness and deep drawability of controlled rolled steels can be improved by controlling the development of austenite textures to strengthen the intensity of {110} <112> component which, in turn, leads to the presence of desirable {332} <113> component in the transformation texture.

Presence of substitutional solutes like Cr, Mo, Mn and Ni, a finer austenite grain size, and a faster cooling rate promote the intensity of the {332} <113> component. {113} <110> component is relatively insensitive to these factors.

In plain C steels rolling below the Ar_3 temperature also leads to the development of a strong {100} <011> texture component.

2.5.2.4 Deformation in α Region

Although deformation of steel in the α region followed

by cooling to room temperature does not lead to any phase transformation but it gives some important and improved mechanical properties. It is sometimes referred to as 'continuum rolling' when it involves successive reductions in the γ, $(\gamma + \alpha)$ and α regions [80]. Recently there has been work on extra low carbon steels [81-85] which, when deformed in the high α range, can yield materials with high R values. It has been found [83] that, for finishing temperatures below 750°C, the intensity of the {111} component increases as the deformatio temperature decreases and the amount of strain increases. This leads to desirable $\bar{R}$ values. Recrystallization carried out after deformation in the α range sharpens the γ fibre component in the α at the expense of the α fibre component [81].

An overall view of the transformation texture components observed experimentally and of the modifications these undergo as a result of rolling in $(\gamma + \alpha)$ and α ranges is depicted schematically in Figure 2.13. The effect of different compositional and processing variables on the relative sharpness of the texture components are also given.

2.6 Microstructure-Texture Correlation during Controlled Rolling

Texture is a statistical property which takes into account a large number of grains and their orientations to get an overall measure. But when we analyze the microstructure it is done on a infinitesimal scale compared to the domain of the textural data. Hardly any significant work has been done till late to correlate the macroscopic texture data and the

corresponding microstructure of the grains. The microstructures of small regions can be analyzed by using a transmission electron microscope and their local orientations determined by using the selected area diffraction (S.A.D.) technique. If a large number of small regions can thus be examined this will yield useful information regarding the correlation of microstructure with crystallographic orientation. These data can then be used in conjunction with the texture data to find out the relationship between the micro and the macro observation. The purpose of the present work is precisely to make such an attempt.
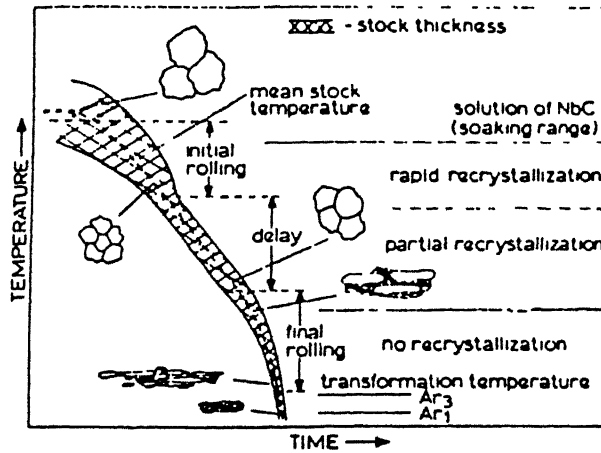
Figure 2.1   Schematic representation of various processes
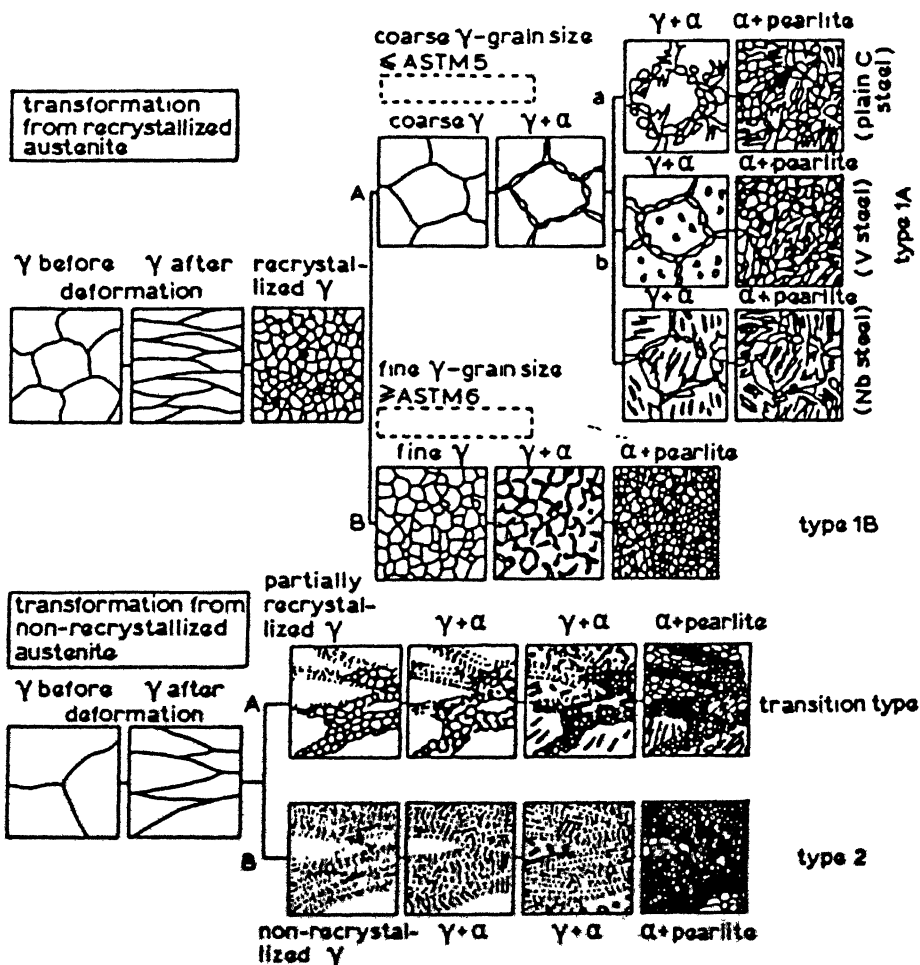taking place during controlled rolling of C-
Mn-Nb steels [21].

Figure 2.2   Schematic diagram of types of austenite-to-ferrite
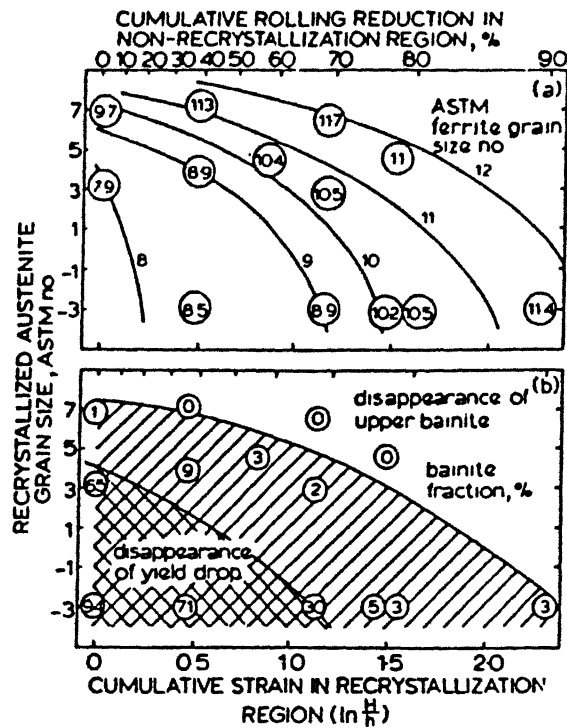transformation for hot-worked steel [21].

Figure 2.3   Effect of recrystallized austenite grain size
and total reduction in non-recrystallization
region on (a) ferrite grain size and (b) upper
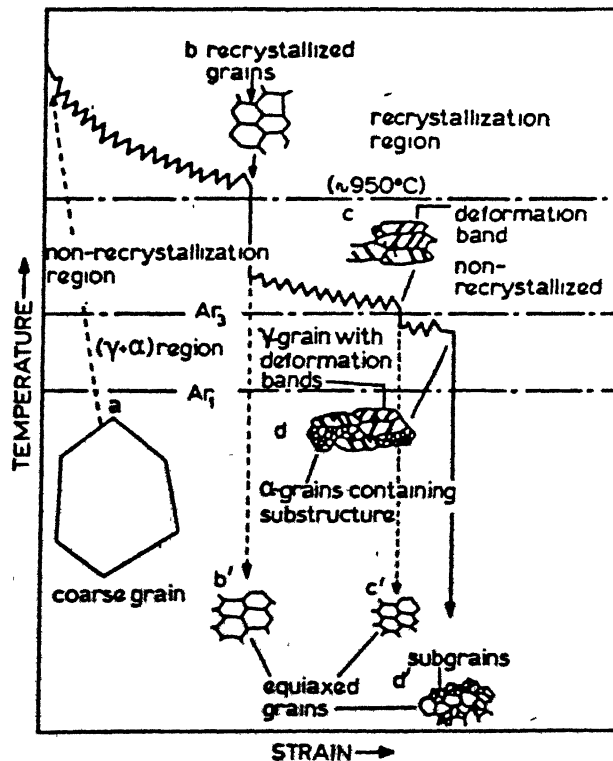bainite fraction in Mn-Nb-V steel [21].

Figure 2.4   Schematic illustration of three stages of
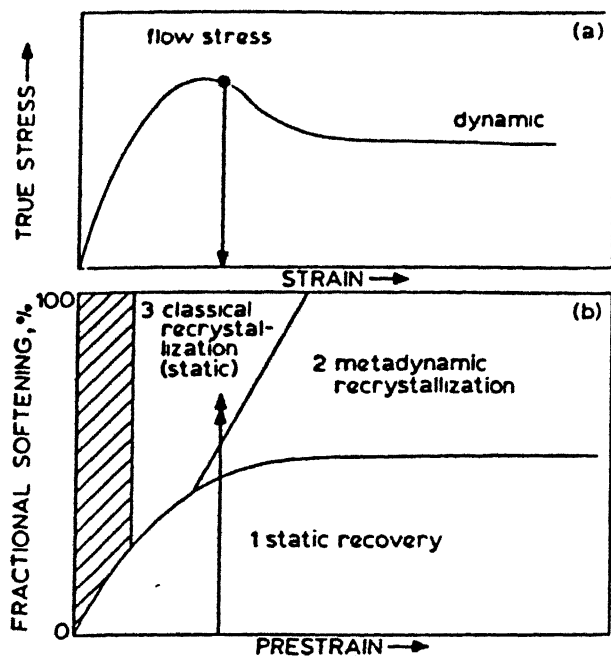controlled-rolling process [21].

Figure 2.5   Schematic represen-
tation of (a) stress-strain curve
and (b) of inter-relation between
three softening mechanisms and of
dependence on strain of softening
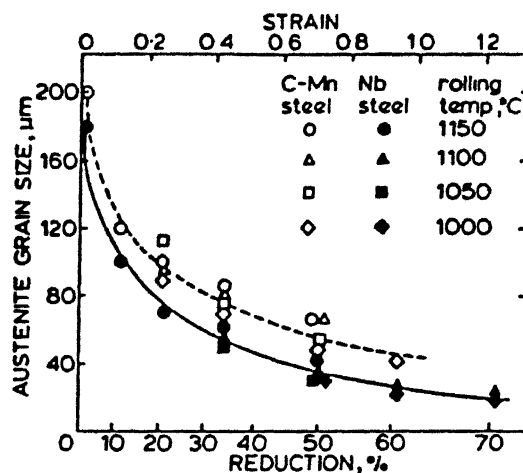proportions attributable to each
mechanism.[21].

Figure 2.6   Influence of
amount of single-pass deform-
ation and deformation temper-
ature on recrystallized auste-
nite grain size in plain C
and Nb steels [21].
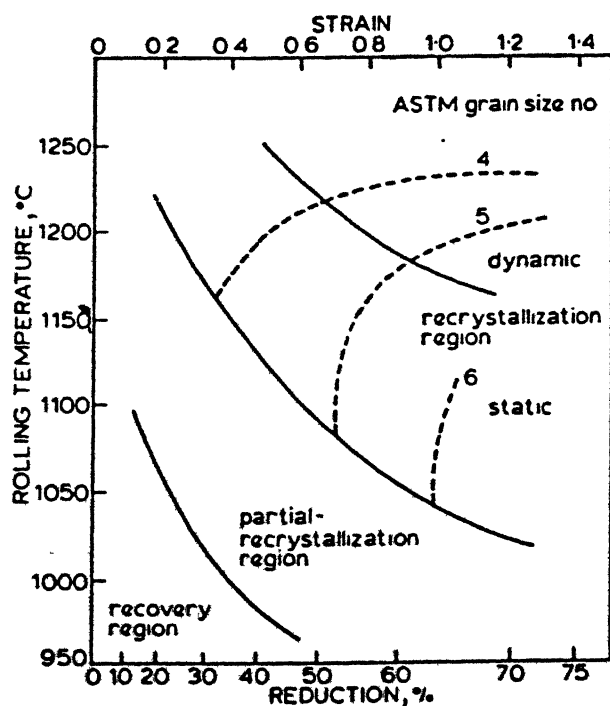
Figure 2.7   Austenite recrystallization and resulting grain
size as function of rolling temperature and
reduction for 0.03% Nb steel; initial grain-size
number was 1.0. [21].
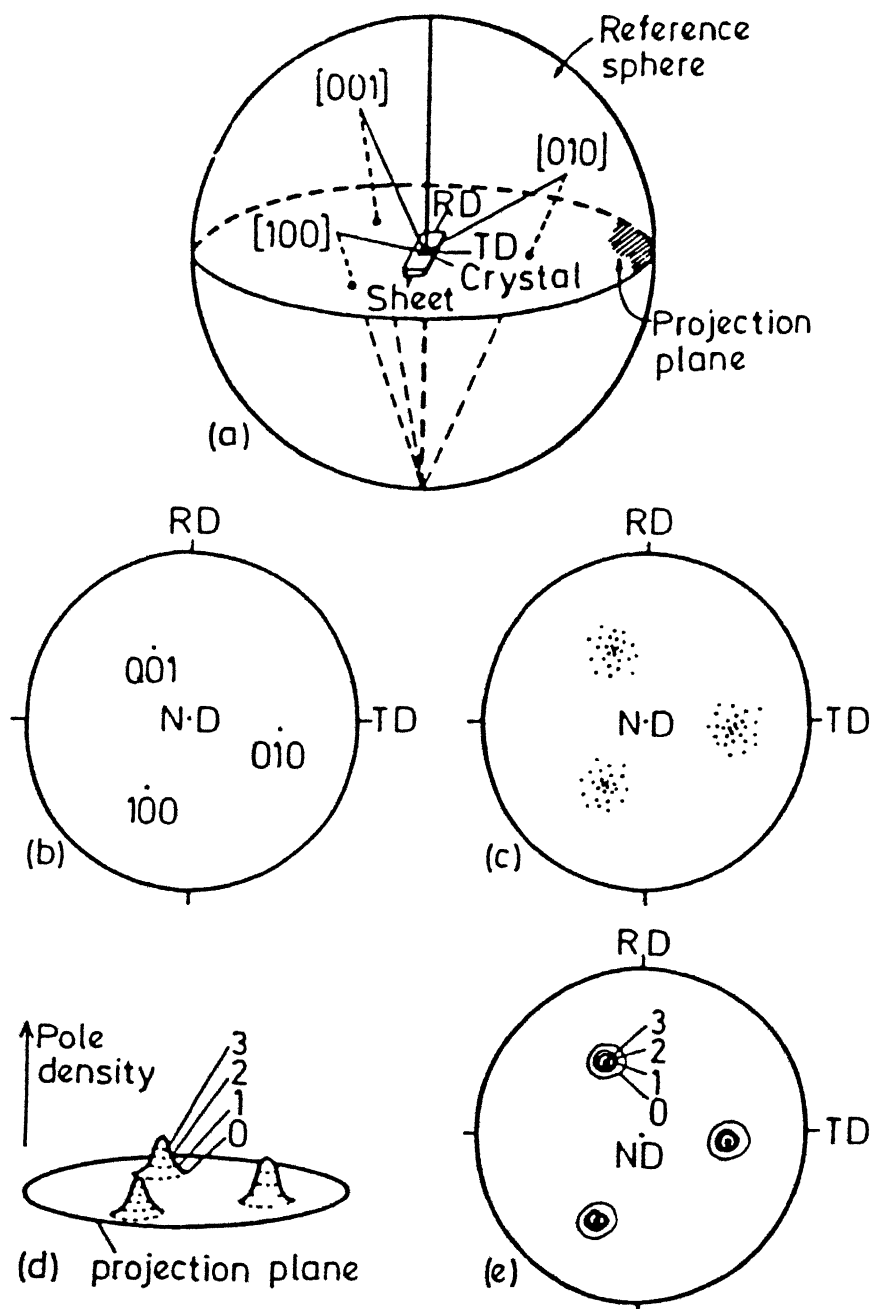
Fig. 2.8 (a) Projection sphere and reference directions,
(b) Projection of poles for a single grain,
(c) Projection of poles from textured grains,
(d) Pole density distribution,
(e) Contour map of pole density.
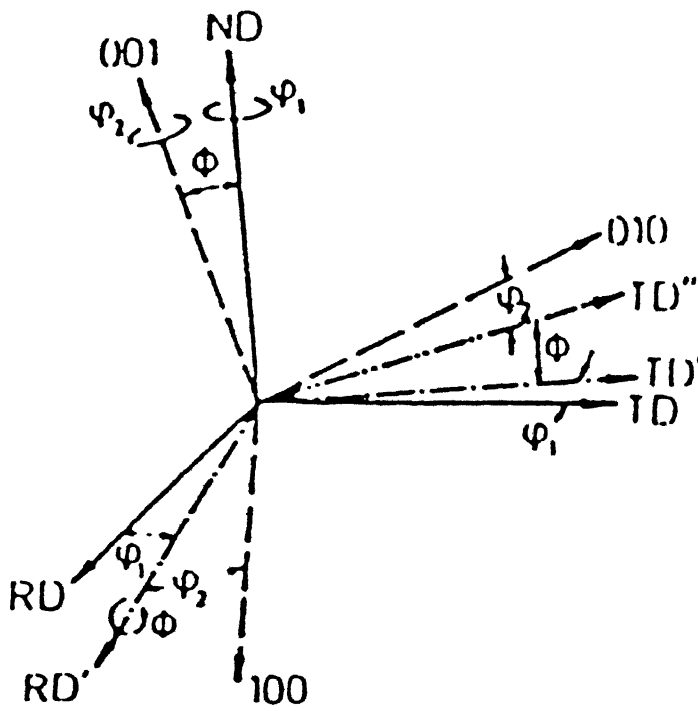
Figure 2.9   Definition of the Euler angles
$\emptyset_1$, $\emptyset$, $\emptyset_2$.
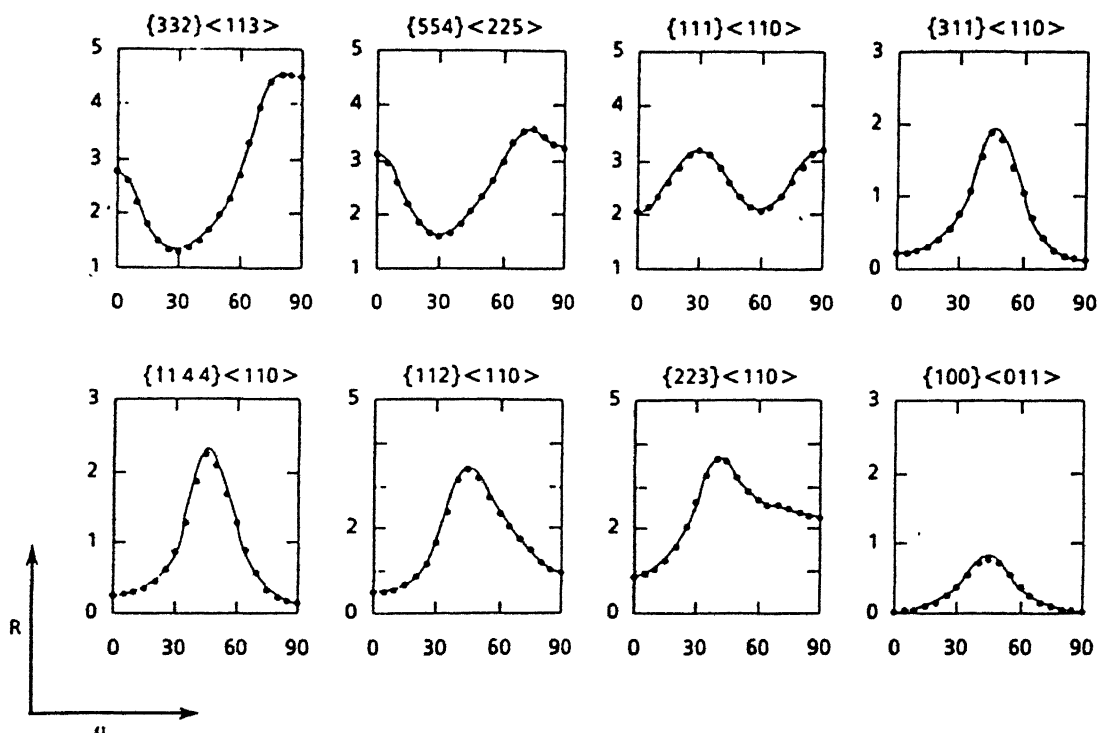
Figure 2.10   Plots of R versus angle α with respect to
rolling direction for selected ideal
orientations.
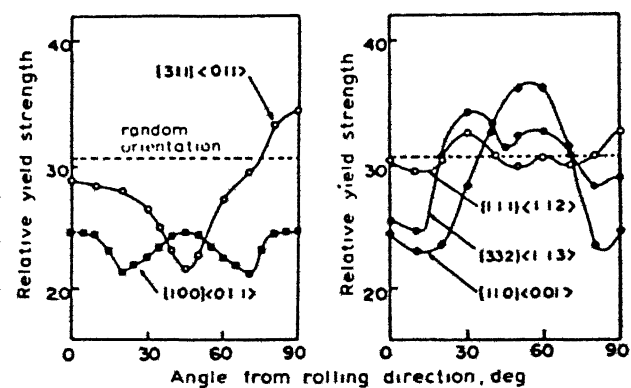
Figure 2.11   Plot of theoretical
relative yield stress vs. angle
from rolling direction for vari-
ous ideal orientations
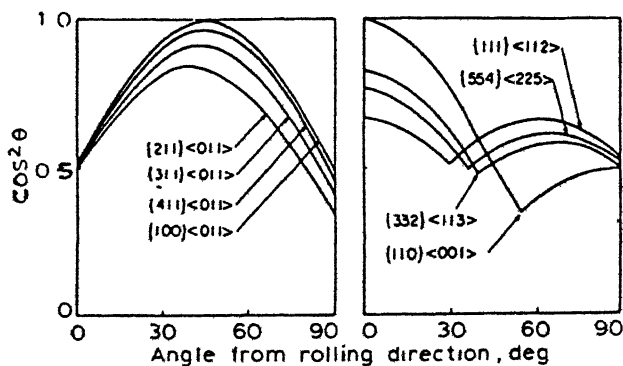
Figure 2.12   Plot of $\cos^2\theta$ vs.
angle from rolling direction
for various ideal orientations

39
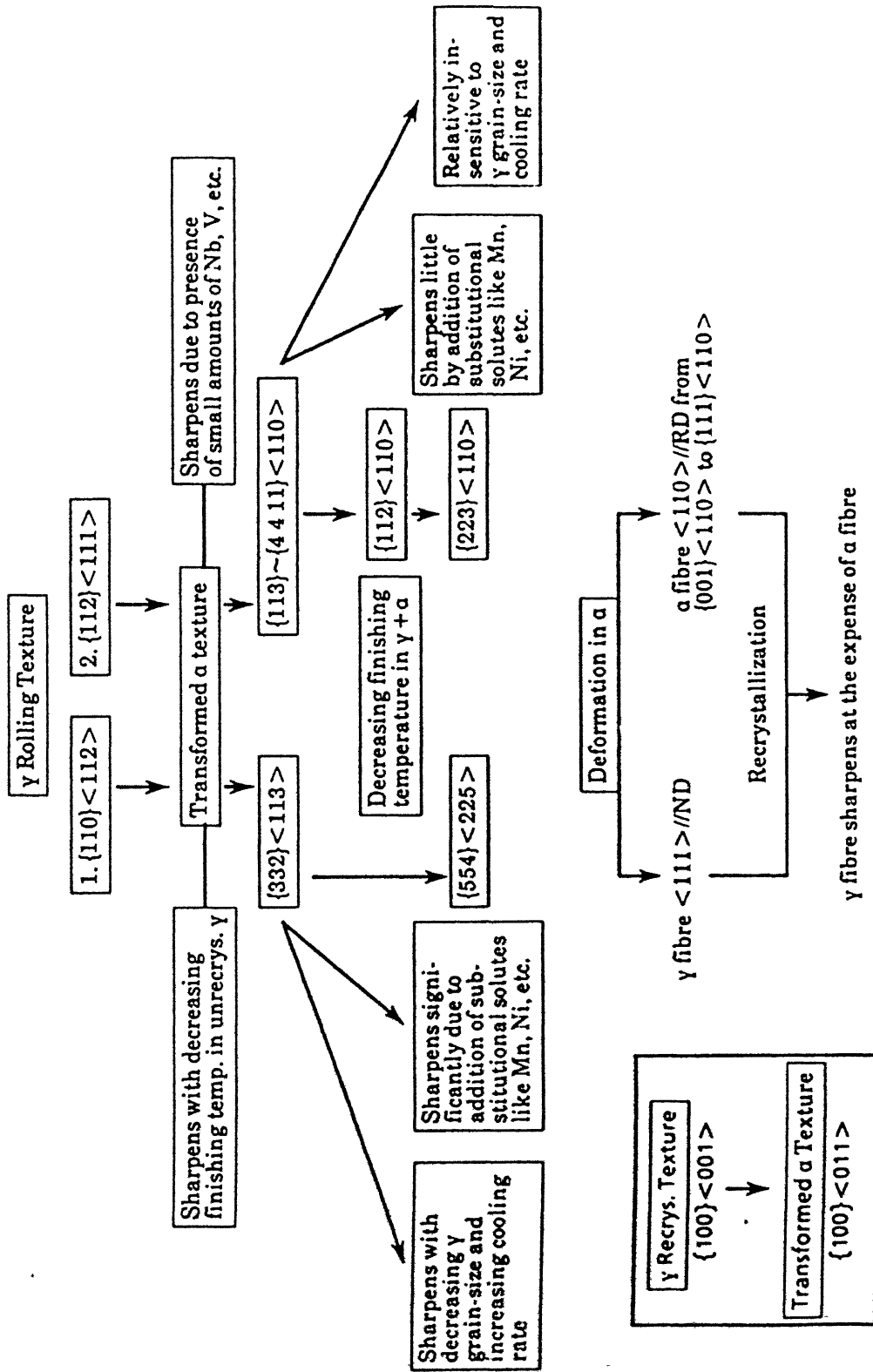
Figure 2.13   Schematic diagram showing effect of compositional and processing variables on the two major components of transformation texture in steel.

Table 2.1 Orientation relationships between γ and α

Orientation relationship	Lattice correspondence relation	Number of alternatives	Total number of variants
Bain (B)	$(001)_\gamma \| (001)_\alpha$	3	3
	$(110)_\gamma \| (110)_\alpha$	1	
Kurdjumov–Sachs (K–S)	$(111)_\gamma \| (011)_\alpha$	4	24
	$(011)_\gamma \| (111)_\alpha$ (twin related variants)	3	
		2	
Nishiyama–Wassermann (N–W)	$(111)_\gamma \| (011)_\alpha$	4	12
	$(112)_\gamma \| (011)_\alpha$	3	

Chapter III

Review of Some Models of Microstructural Evolution during the Hot Deformation of Steels

3.1 Introduction

Numerical models of the deformation characteristics of metals have traditionally been validated by the comparison of computed and measured values of external parameters like changes in shapes or the forces required for those shape changes. Isolated temperature measurements have been used to verify calculated temperature profiles. The changes in microstructure within the metal are also vitally important in hot working operations.

The microstructural changes involve competing work hardening and softening processes, the relative extents of which determine the flow stress and therefore the operating loads and conditions of metal flow during the working operation. Also, the final room temperature properties, particularly final grain size, determined by recrystallization and grain growth, are largely determined by the microstructure developed during hot working.

Recently, modelling of microstructural evolution during steel processing has attracted extensive research. Mainly, two different approaches have been adopted for the problem of simulating the thermomechanical processing of steels: (1) Flow stresses, and from them, microstructural behaviour of a given material, are determined under deformation conditions

of varying complexity that are closely related to industrial processing schedules [86-88], and (2) Detailed and separate characterization of the most relevant phenomena (recovery, recrystallization, grain growth) is used to derive a set of analytical, semiempirical relationships, aimed at describing all aspects of microstructural evolution for a given type of material under a wide range of deformation conditions; and this forms the basis for a model of microstructural evolution [89-91]. The second approach is assumed to be far more general with respect to the applicability of the models, in terms of both the type of materials and the deformation conditions.

Two major models of microstructural evolution in steels, which have been presented in the literature by two groups [92, 93-97] form the main basis for the present review. Different investigations performed on the basis of these models have been discussed. An evaluation of similar two models by another group [98] has also been reviewed.

3.2 Model by J.H. Beynon, A.R.S. Ponter and C.M. Sellars

3.2.1 Approach   for Computation

Steady state hot rolling of wide flat strips is the process that has been modelled. Plain strain conditions were assumed, which simplified the model to a two-dimensional problem.

A Eulerian finite element model [99, 100] for temperature, strain rate and strain distribution within the roll bite during rolling has been combined with a finite difference model [101-103] for temperature distribution and microstructural

evolution between deformation passes . These inter-pass periods, during which continuous cooling of the stock occurs, are extremely important for the development of microstructure by the processes of recrystallisation and grain growth.

3.2.2 Microstructure Evaluation

Barbosa [104] determined the kinetics of static recrystallization and grain growth for 316L stainless steel. The grain growth was found to be slow under the conditions used. So the relevant equations are mainly for recrystallization. Time for 50% recrystallization ($t_{0.5}$, in secs.) is given by the following empirical relationship

$$t_{0.5} = 4 \times 10^{-15} \, z^{-0.88} \, \varepsilon^{0.6} \, d_o^{1.33} \, \exp\{\frac{475000}{RT}\}$$

$$\text{for} \quad \varepsilon \leq \varepsilon^*$$

where ε^* is the strain for the onset of dynamic recrystallization, but this is not attained for the conditions considered. ε is the effective strain, d_o is the grain size of the metal before recrystallization (μm), T is the temperature after deformation (K) and R is the gas constant (8.314 J $\text{mol}^{-1}\text{K}^{-1}$), z is the Zener Holloman parameter.

The fraction recrystallized (X) follows an Avrami equation

$$X = 1 - \exp\{1 - (\ln 2)(t/t_{0.5})^k\}$$

where k is a constant, found [104] to be 0.6, and t is the time for the fraction X to recrystallize. The resulting recrystallized grain size (d_{rex}, in μm) is given by

$$d_{rex} = 470 \, d_o^{0.3} \, z^{-0.1} \, \varepsilon^{-1}$$

which is achieved when recrystallization is just complete. For partial recrystallization the present size of the recrystallized grains, d_r, is given by [92]

$$d_r = x^{1/3} \, d_{rex}$$

and the resulting mean grain size for the microstructure is

$$d = x^{3/4} \, d_{rex} + (1 - x)^2 \, d_o$$

3.2.3 Different Investigations Based on this Model

The hot rolling of austenitic stainless steel has been modelled for comparison with laboratory results [92].

Initial work by Barbosa [104] consisted of comparisons between the evolved microstructure predictions by this model and those observed metallographically. The steel used had the composition

wt. %	C	Cr	Ni	Mo	Mn	Si	N
Alloy A	0.024	16.70	12.20	2.63	1.50	0.29	0.039

These were reheated to $1160^{\circ}C$ and given three phases of 25% reduction each with 15 secs. between passes . The results of the computer predictions for the first pass of this schedule are given in Figures 3.1 and 3.2. These show the distributions of temperature, strain and Zener-Hollomon parameter during the pass, and the resulting microstructure developed in the interpass period.

These predictions were checked by metallographic examination of the stock at the mid-point between surface and centre. Just before pass two, this showed two populations of grain size were present, with a mean grain size that compared well with the predicted value [92].

Gorman [105] carried out investigation on the effects of different roll pass geometries on gradients in recrystallization kinetics using steel of composition

wt. %	C	Cr	Ni	Mo	Mn	Si	N
Alloy B	0.017	16.30	12.20	2.29	1.83	0.58	0.077

Variations in the value of the ratio of roll contact length to mean thickness were achieved by the use of constant roll radius and varying the initial geometry of slabs and the rolling reduction. The ratio is given by the following expression

$$r = [\frac{R \, \Delta h}{h_o h_f}]^{1/2}$$

where R is the roll radius, h_o and h_f are the initial and final stock thicknesses respectively, and Δh is the reduction in stock thickness.

The rolled slabs were quenched and cut into pieces and annealed for various times. The fraction recrystallized at various depths through the thickness was measured to determine whether a gradient in recrystallization was present. The result of Gorman's work, given in Table 3.1, show that gradients

in recrystallization kinetics exist in the form predicted by
the model. However, they appear to a lesser extent than expec-
ted from the model. Lower values of r are required to produce
gradients of the form shown in Figure 3.3.

Another recent work done by McLaren et al [106] has
been performed on the basis of the inferences drawn from Gorman's
work. It was proposed to put extreme rolling condition to get
a significant gradient in recrystallization. A slab of steel of
following composition of original thickness 51 mm was rolled at

wt. %	C	Cr	Ni	Mo	Mn	Si	N
Alloy C	0.022	17.11	11.62	2.56	1.61	0.36	0.028

1000°C to a final thickness of 39 mm, giving a reduction of 22%.
The value of the ratio r is 0.63.

The slab was quenched after rolling and cut into pieces
to be annealed for various times at 1000°C. The results of
these measurements for an annealing time giving ≈20% recrystal-
lization are shown in Figure 3.4 compared with the predictions
of the model [97].

The results confirm that the gradient is present, but
to a lesser extent than predicted, and that the maximum is
further from the surface than that in the model.

The probable reason suggested [106] for the differences
in the results measured and those predicted by this model is
that work hardening is not taken into account by the model.

Work hardening increases the flow stress with strain, and is more pronounced in those regions where temperature is lowest. The strain is therefore expected to spread more homogeneously through the stock. This would account for the smaller measured gradients in fraction recrystallized than those predicted. The work hardening of the areas beneath the surface which are initially strained more as a consequence of the flow constraints imposed by the rolls leads to the shift of the strain peak at exit further towards the centre of the stock.

The various results indicate that the inclusion of work hardening together with the strain rate and temperature dependence of flow stress in the constitutive equations employed in the model will be necessary to obtain agreement with observations.

3.3   Model by T. Senuma, H. Yada and Co-workers

3.3.1   The Mathematical Model

A comprehensive model has been developed for predicting microstructural changes and some resulting mechanical properties of low carbon steels [93-97]. The model is especially suited for the application to hot strip mill because it took due consideration of high-speed successive hot deformation and steels with high transformation rate. This has been extended to plain carbon steels alongwith some alloy steels. The application to niobium bearing steels have also been performed [107].

Models of some basic metallurgical phenomena have been used to get the model for the whole process as shown in Figure 3.5.

The initial state model predict an austenite grain size after reheating. This serves as the initial grain size for further hot deformation.

The hot deformation model formulates all the elements of metallurgical phenomena such as dynamic and static recrystallization, dynamic and static recovery, and grain growth. This model includes all the effect of previous deformation on recrystallization in the subsequent deformation in terms of the residual dislocation density. So it can be applied to the multipass deformation. Plain carbon steels with a wide range of chemical composition can be subjected to this model due to insignificant difference in their recrystallization behaviour. For alloy steels, which contain the alloying elements retarding the recrystallization, like niobium, only modification of some of the parameters was needed.

A transformation model had initially been developed for the transformation from austenite to ferrite, pearlite and/ or bainite, of low carbon steels [94]. Recently the model has been extended to be applied to plain carbon steels alongwith some alloy steels.

Two types of basic equations shown in Table 3.2 have been used. One is for the case of nucleation and growth (NG) and the other for the case of saturated nucleation sites (SS). Ferrite transformation calculation starts when the temperature drops to the equilibrium temperature, Ae_3, calculated from thermodynamic parameters. Its progress has been calculated as the NG at the early stage and then the SS at the later.

Pearlite transformation is generally assumed to start when the carbon content in γ meets the extrapolated A cm line in the phase diagram. But below 960 K the pearlite transformation is found to start before the above condition is satisfied, which may be due to the distribution of carbon between ferrite and austenite at the γ/α phase boundary and correction for this has been incorporated. NG equations are used for the calculation of pearlite transformation. Bainite transformation was assumed to conform to SS without the concentration of carbon into austenite. For the bainite start temperature, B_s, the following equation is used

$$B_s(k) = 990.5 - 425[\text{wt. \% C}] - 42.5[\text{wt. \% Mn}]$$

The effects of chemical composition (C, Si, Mn, Ni, Cr, Cu) on transformation kinetics are included in terms of the change of Ae_3, nucleation rate and growth rate calculated by using thermodynamic parameters.

The ferrite grain size is here calculated with the 5% ferrite transformation temperature, $T_{0.05}$, and the final ferrite fraction, X_F, as

$$d_\alpha \ (\mu m) = \left[5.51 \times 10^{10} \ d_\gamma^{1.75} \exp\left(-\frac{21430}{T_{0.05}}\right) X_F \right]^{1/3}$$

The effect of austenite grain size has been explicitly considered in the model, as in Table 3.2. The effect of the stored strain was taken into consideration by using the effective austenite grain size, d_γ^{eff}, instead of d_γ

$$d_\gamma^{eff} = d_\gamma / (1 + 10^{-11} \ \rho^{1.154})$$

where ρ (in cm^{-2}) is the calculated residual dislocation density just before transformation starts.

3.3.2 Structure-Property Relationship

Irvine and Pickering showed that the tensile strength of ferrite-pearlite steel and bainitic steel was determined from the transformation temperature of steels [108]. They had only changed the composition keeping the microstructure mostly uniform. In modern processing of steel they often have mixed microstructure. It has been shown by experiments that even in such steels the hardness of ferrite and bainite is determined by the transformation temperature as shown in Figure 3.6 [95]. In higher carbon steels, as seen in Figure 3.7, the hardness depends on carbon content and transformation temperature. It can be explained that the dispersion hardening by cementites substantially contribute to hardness of bainite at higher carbon contents. Figure 3.7 also shows an increase in hardness with increasing transformation temperature above 943 K which is due to the carbon content enriched in austenite close to the value on the equilibrium condition. From these results the microhardness, H_v, was formulated as

$$H_v = X_F H_F + X_P H_P + X_B H_B$$

$$H_F = 458.5 - 0.357 \, T_F + [50\% \, Si] + a.d_\alpha^{-1/2}$$

$$H_P = 604.0 + 645.5 \, C_\gamma - (0.538 + 0.5 \, C_\gamma)T_P + 50[\% \, Si]$$

$$H_B = H_P$$

where X is the fraction transformed, d_α (in mm) the ferrite grain size, [% Si] the silicon content in wt. %, and T(k) the average transformation temperature of each microconstituent. The subscripts F, P, B denote ferrite, pearlite and bainite respectively. The constant, a, was estimated as 2.55. C_γ is the carbon content enriched in austenite.

3.3.3 Different Investigations Based on this Model

Wire rod rolling was conducted in practice according to schedule shown in Table 3.3. The results observed and calculated are also tabulated. In case B the material was fully recrystallized in a short time after final deformation even if the final reduction was small and the deformation temperature was low. This recrystallization behaviour was predicted by the present model. This demonstrates the important role of the residual strain in the recrystallization process and indicates that its accurate determination is essential for the prediction of the microstructural change in the high speed continuous rolling processes.

Another work was done on 0.1% C - 0.3% Si - 1.2% Mn steel. The effect of dislocation density and austenite grain size on the temperature at 5% ferrite fraction during cooling is provided in Figure 3.8. This figure indicates that the residual dislocation density remarkably accelerates the increase of transformation temperature of steel with a larger austenite grain size.

A prediction of strength of hot rolled steels was per-
formed. This was calculated on the assumption that a linear
relationship between hardness and strength exists, i.e. T_s (in
MPa) $= a.H_v$ where a is the constant. The tensile strength of a
strip hot rolled in a production mill was measured and compared.
Table 3.4 shows the chemical composition of steel used and
processing conditions in the production mill. Figure 3.9 com-
pares the strengths calculated with those measured.

Niobium bearing steels was used in another investigation
for prediction of strength. Nb in solution affects recrystalli-
zation behaviour of austenite significantly. This effect was
quantitatively dealt by Akamatsu et al [109]. Their result
showed that the apparent activation energy for static recrystal-
lization below the solution temperature of NbC was twice as
high as that for ordinary steels. Fujioka et al [110] showed
that only niobium in solution charged the kinetics of ferrite
and pearlite transformation significantly, and bainite trans-
formation was insensitive to Nb.

The models including the above effects of Nb was comb-
ined with a precipitation model of NbC in austenite, to predict
the strength of hot-rolled Nb bearing steels. Figure 3.10
shows the calculated and measured tensile strengths of hot-
rolled 0.11% C - 0.10% Si - 0.75% Mn steel with different nio-
bium contents. In the calculation, the precipitation of NbC in
ferrite is not dealt with as a low holding temperature is used.
The compatibility between the strengths calculated and measured
indicates that the change in strength of steel is caused by the

change in microstructure due to niobium. For higher cooling

temperature, the effects of precipitates in transformation

products on strength should be considered.

So it can be seen from the various results that the

microstructural evolution of steels calculated and the strength

calculated from the resultant microstructure, using this model,

showed good congruence to those observed. This model is being

put into practical use.

3.4 An Evaluation of Two Similar Models of Microstructure Evolution Reviewed

Two models of microstructural evolution in steels, have

been examined for their accuracy of prediction of the occurrence

of recrystallization and the final austenite grain size [98].

The two models have been presented by the group of Sellars at

Sheffield [90-102] and by the group of Yada in Japan [89, 111,

112]. They are very similar models to the ones explained in

the previous sections. They have been tested against experi-

mental data obtained in single-step, hot compression testing

of carbon steels. A carbon steel billet of the composition

0.44% C, 0.9% Mn, 0.28% Si, 0.023% S, 0.028% P, 0.07% Cu, 0.03%

Ni, 0.06% Cr, 0.011% Sn, 0.015% Mo, 0.003% Al (referred to as

1045 steel) and another steel bar of composition 0.21% C, 0.58%

Mn, 0.09% Si, 0.01% S, 0.02% P (referred to as 1020 steel) were

machined to axisymmetric compression specimens. The set of

experimental conditions used in the experiments are shown in

Tables 3.5 and 3.6.

The specimens prepared for metallographic examination

after deformation were used to calculate austenite grain sizes
by linear intercept method keeping the probable errors to $\pm$10%.
Austenite grain size of initial materials were also calculated.

3.4.1 The Models of Microstructure Evolution

Sellars model [90, 102] provided explicit equations for
the calculation of statically recrystallized volume fractions
(X_{SR}) and grain sizes (d_{SR}), whether or not preceded by dynamic
recrystallization. This model also gives two equations for the
calculation of austenite grain growth, at temperatures higher
or lower than 1000°C. The recrystallized and non-recrystallized
volumes are treated independently of each other in the cases of
partial recrystallization.

Yada model [89, 111, 112] assesses initially the occur-
rence of dynamic recrystallization and performs calculations
for the volume fractions (X_{DR}) and grain sizes (d_{DR}) of the
dynamically recrystallized material. Equations for recovery,
statically recrystallized volume fractions and grain sizes have
been provided. An elaborate procedure, in terms of a residual
deformation and an average grain size has been dealt for the
case of partial recrystallization. Kinetics of grain growth of
recrystallized grains have also been covered and equations have
been provided.

Figures 3.11(a,b) depict the general procedures that
were used in the evaluation regarding the calculation of recrys-
tallized volume fractions and austenite grain sizes, following
the methods suggested by the two models. A time of 2 secs. has

been indicated in some steps, allowing for the time elapsed between the end of the deformation and the quenching to near room temperature in the experiments.

3.4.2 Comparison of Computed and Experimental Results

The austenite grain sizes found in the deformed compression specimens alongwith the grain sizes of undeformed specimens have been provided in Tables 3.5 and 3.6. It can be seen that recrystallization has occurred in the majority of the specimens used.

Tables 3.7 and 3.8 provides a comparison between the observed and calculated final austenite grain sizes. The prediction of static recrystallization to occur was also given with the corresponding actual observations of its occurrence in these tables.

In the case of the 1045 steel, the models give nearly accurate values of grain sizes, to that observed, in about one third of the experiments. But some 40% of the predictions are too far from the observed values and the remaining are somewhere in between these two extremes. The predictions of occurrence of static recrystallization are correct in about 80% of all the cases for both the models.

In the case of 1020 steel, accurate grain estimates are provided in about 50% of the predictions for Sellars model compared to only about 25% in the case of Yada model. The former model also yielded a lower fraction of way-off grain size estimates (about 25%) as compared to the latter (about 45%)

However, the qualitative predictions of occurrence of static recrystallization by both models are about the same.

The above results indicate that the two models predict accurately the development of partial or complete static recrystallization under most of the condition used in the tests, but the estimates of the resulting austenite grain sizes had an even chance at turning out right or wrong.

It has been suggested that it may be necessary to improve the current knowledge of recrystallization (specially the dynamic recrystallization) in carbon steels with an emphasis on the recrystallized austenite grain size and its subsequent growth, as well as on any composition dependence of these phenomena, to get an effective improvement in modelling the evolution of austenite microstructures in carbon steels.
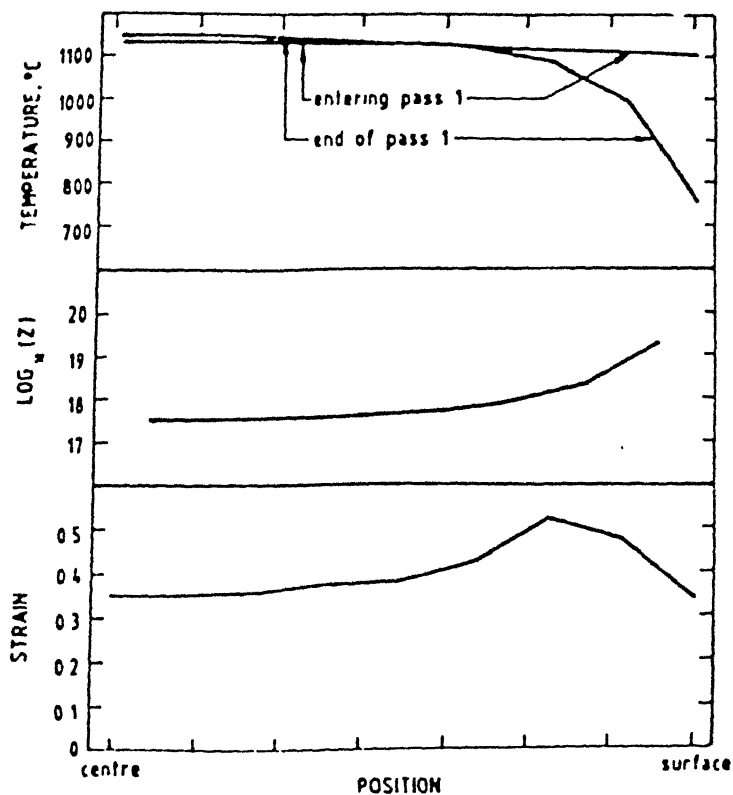
Figure 3.1   Predicted thermomechanical state of a slab of
steel A immediately after a pass of 25% reduc-
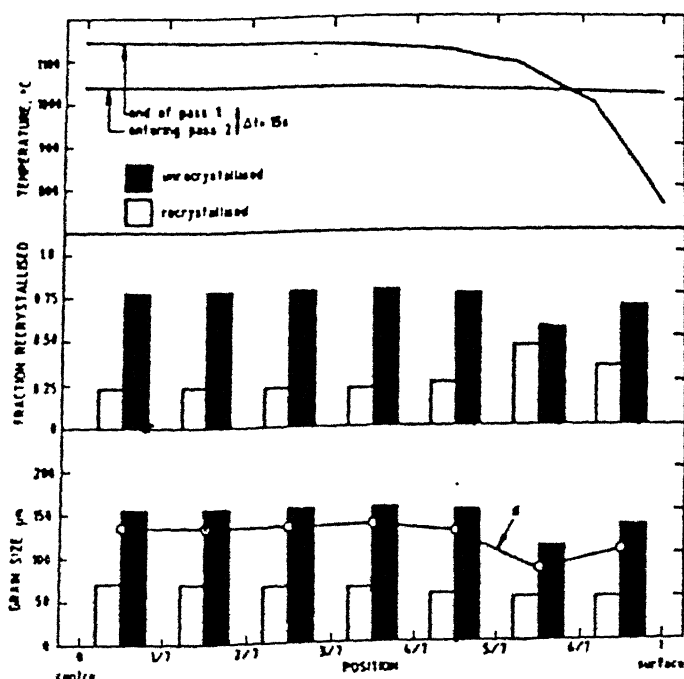tion from original thickness 25 mm after rehea-
ting to 1160°C

Figure 3.2   Predicted microstructural state of a slab of
steel A 15 seconds after the pass shown in
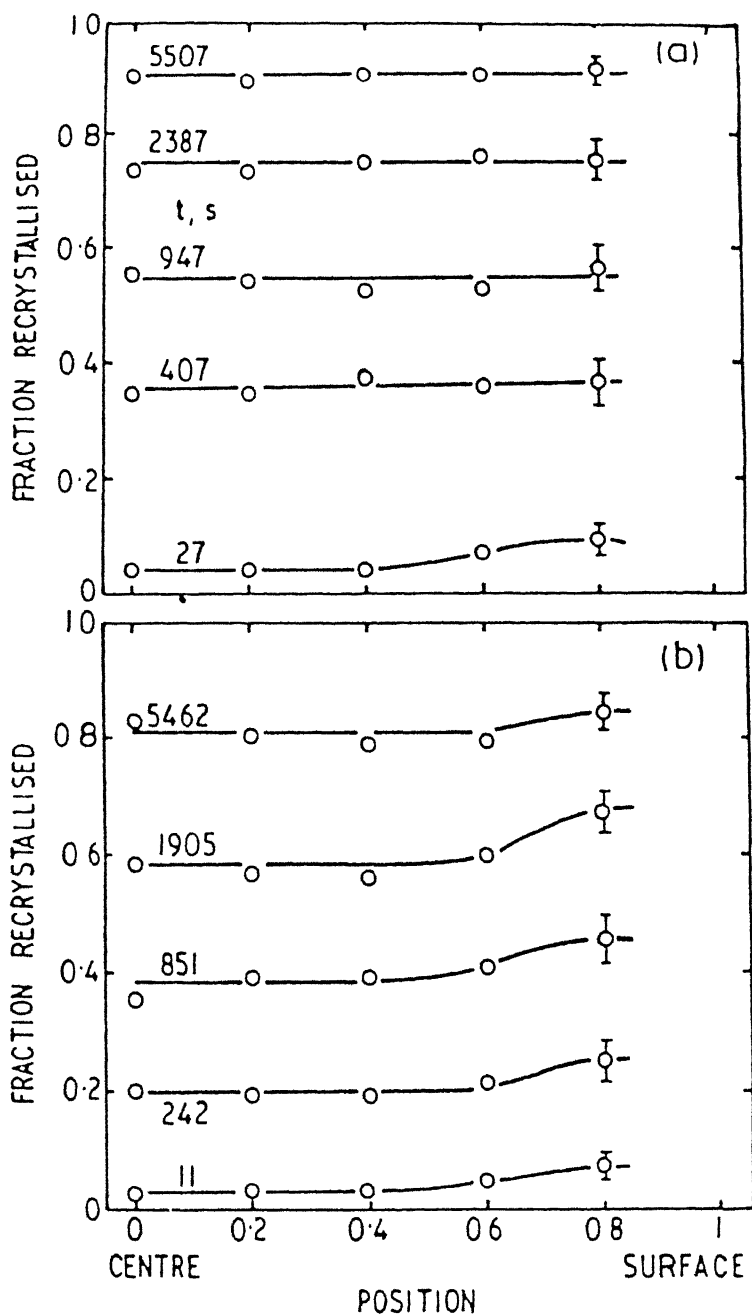Figure 3.1. Original grain size 200 μm

Figure 3.3   Measured distribution of recrystallization in slabs of steel B, reheated to 1100°C, rolled at 1000°C, quenched and annealed for varying times (t) at 1000°C
(a) Original thickness 27.5 mm, 20% reduction.
(b) Original thickness 36 mm, 10.75% reduction.

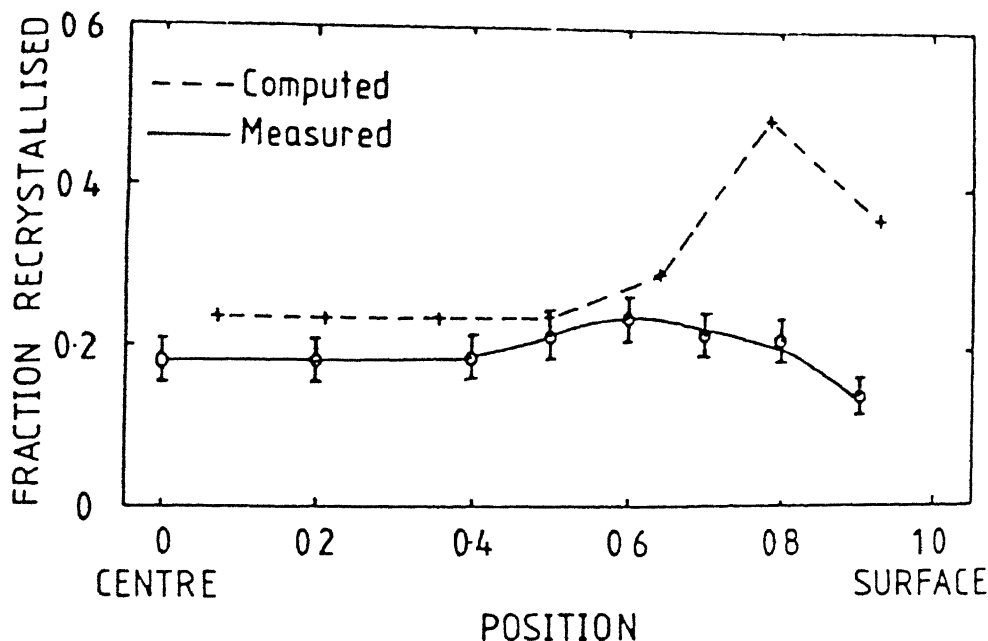Figure 3.4   Comparison between predicted (by model) and measured
distributions of recrystallization in a slab of steel
C, reheated to 1100°C, rolled at 1000°C, quenched and
annealed at 1000°C for an equivalent time of 86 seconds
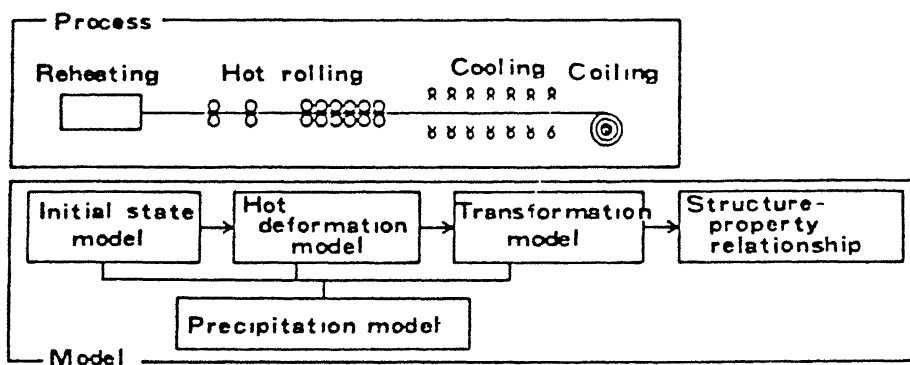
Figure 3.5   Concept for the mathematical modelling.
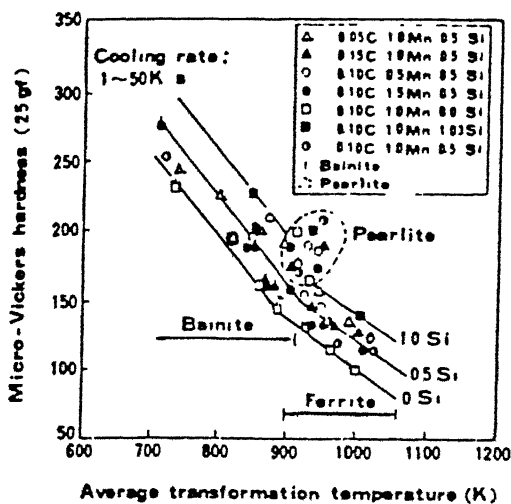
Figure 3.6   Relationship between the measured micro-hardness of
each microconstituent and its calculated average trans-
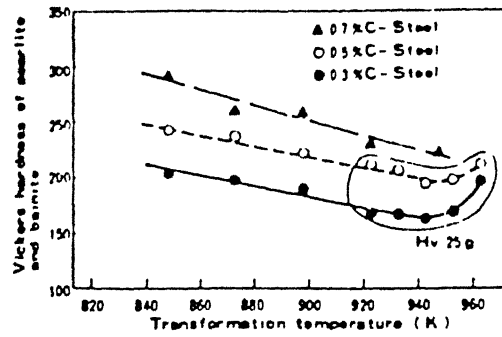
Figure 3.7   Effect of carbon content on the relationship between hardness and transformation temperature of high carbon steels.
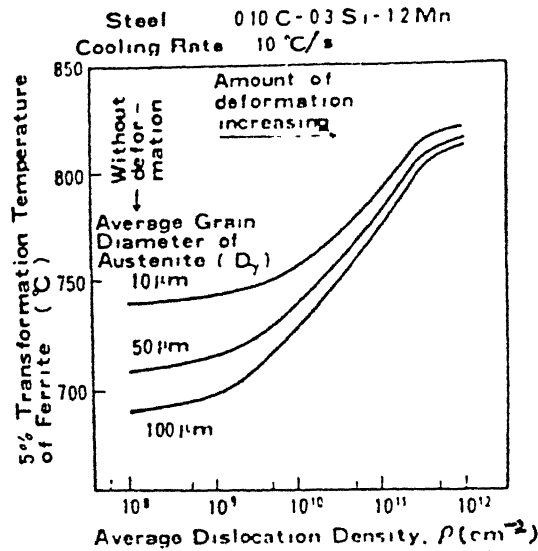
Figure 3.8   Effects of austenite grain size and average dislocation density on 5% transformation temperature of ferrite.

Figure 3.10   Effect of niobium content on tensile strength.

Figure 3.9   Comparison of the tensile strengths calculated to those observed. The sample numbers
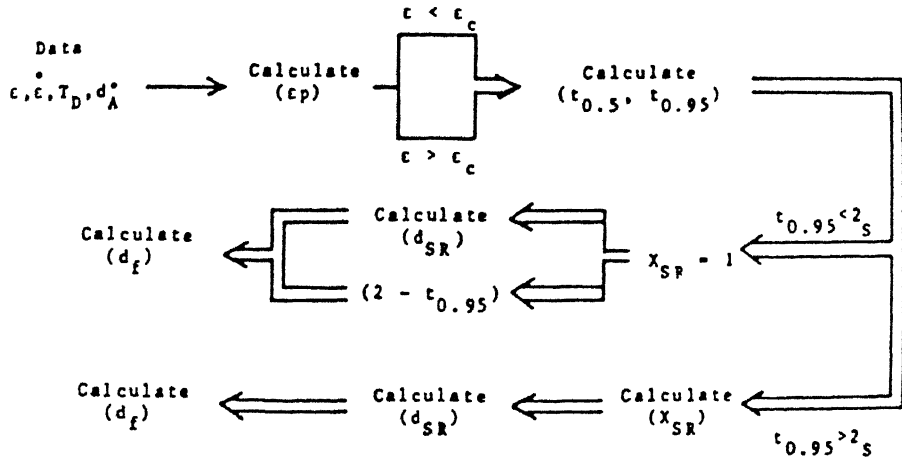
(a)

(b)

Figure 3.11   Schematic representation of the calculations involved by using (a) Sellars model and (b) Yada model.

Table 3.3

lling schedule of wire-rods and resulting austenite grain size
asured and calculated

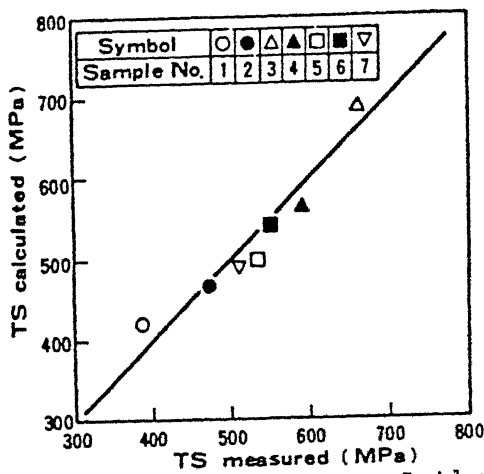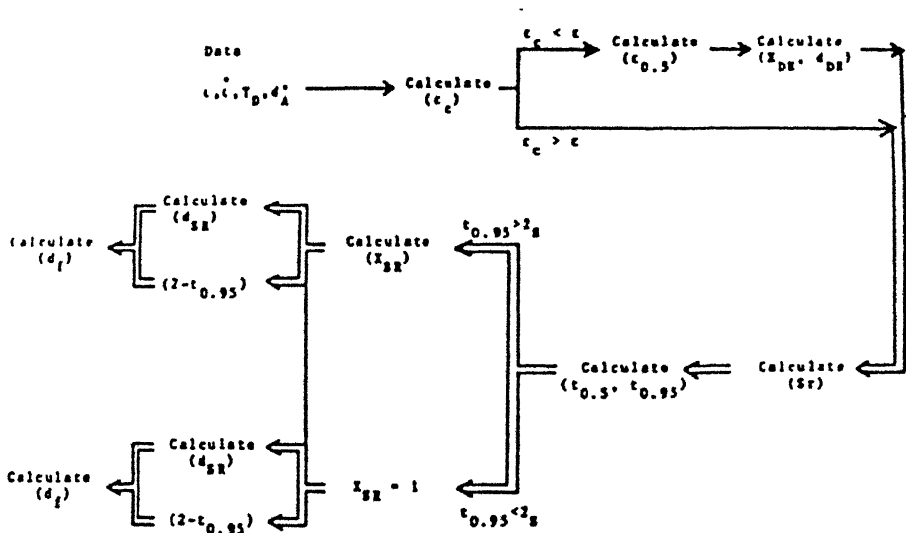| t	D₀		Intermediate train			Finishing train						grain size (μm)	
			14th	15th	16th	17th	18th	19th	20th	21st	22nd	measured	calculated
	50	ℓ	0.285	0.136	0.254	0.124	0.243	0.082	0.102	0.108	0.054	15	17.2
		$\dot{\epsilon}$ (1/s)	38	40	72	72	102	96	158	200	126		
		T(C)[1]	900	910	920	930	940	950	960	970	980		
		Time to next stand(s)	0.63	0.78	1.75	0.23	0.17	0.15	0.13	0.12	0.21		
[2]	18	T(C)[1]	790	790	790	785	785	785	780	780	780	9.3	10.2

1) calculated temperature   2) speed of wire rod is halved. ℓ is the same as test A

Table 3.4

hemical composition of steels used and processing conditions in
roduction hot rolling mill

Sample No	Chemical composition (wt%)							FT (K)	CT (K)	Thickness (mm)
	C	Si	Mn	P	S	Aℓ	N			
1	0.09	0.01	0.44	0.015	0.005	0.019	0.0017	1153	873	3.2
2	0.15	0.01	0.51	0.013	0.007	0.033	0.0020	1163	843	3.2
3	0.17	0.45	1.40	0.014	0.005	0.030	0.0038	1173	773	3.2
4	0.17	0.45	1.40	0.014	0.005	0.030	0.0038	1143	873	3.2
5	0.17	0.45	1.40	0.014	0.005	0.030	0.0038	1153	953	3.2
6	0.17	0.45	1.40	0.014	0.005	0.030	0.0038	1183	903	2.5
7	0.13	0.27	1.07	0.015	0.002	0.034	0.0032	1073	873	6.0

T_D (ºC)	ϵ	d_f (um)	$d^{\underline{o}}$ (um)/T_A(ºC)
1270	.02	436	336/1320
1294	.06	364	same
1270	.12	186*	same
1265	.37	135*	same
1246	.83	129	same
1245	.94	125	same
1200	.02	196	190(127)/1260
1196	.04	168*	same
1200	.07	129*	same
1220	.17	98	same
1198	.43	86	same
1200	.70	63	same
1200	1.09	68	same
1095	.01	177*	121(195)/1150
1100	.05	121	same
1098	.05	144*	same
1094	.12	86	same
1093	.34	69	same
1102	.63	34	same

T_D- deformation temp.; ϵ - deformation; d_f-
final austenite grain size; $d^{\underline{o}}$- initial grain
size; T_A- austenization temp.
* indicates duplex grain size (minor compo-
nent in parenthesis)

Table 3.6

Deformation conditions and austenite grain sizes for the
1020 steel

T_D (ºC)	ϵ	d_f (um)	$d^{\underline{o}}$ (um)/T_A(ºC)
1200	.37	76	202/1270
1200	.41	93	same
1200	.61	70	same
1112	.84	51*	115/1170
1100	.39	62	same
1100	.22	67	same
1085	.32	71	same
1017	.75	50	same
1003	.39	44*	78\1050
980	.62	33	same
939	.36	41*	69/950
903	.37	51	same
902	.60	38*	same

Meaning of symbols as in Table 3.5

Table 3.7

Comparison of experimental observations and models' predictions for the 1045 steel

Final Austenite Grain Size (um)			Occurrence of Static Recrystallization		
Obs.	NKK	Sellars	Obs.	NKK	Sellars
436	336	336	no	no	no
364	333	340	no	p	p
186	201	270	p	p	p
135	100	85	p	c	c
129	51	83	c	c	c
125	48	83	c	c	c
196	190	190	no	no	no
168	138	190	p	p	no
129	129	120	p	p	p
98	94	99	c	c	c
86	64	74	c	c	c
63	50	75	c	c	c
68	38	75	c	c	c
177	195	195	p	no	no
121	121	121	no	no	no
144	121	195	p	no	no
86	116	117	c	p	p
69	70	56	c	c	c
34	39	58	c	c	c

p - partial; c - complete

Table 3.8

Comparison of experimental observations and models' predictions for the 1020 steel

Final Austenite Grain Size (um)			Occurrence of Static Recrystallization		
Obs.	NKK	Sellars	Obs.	NKK	Sellars
76	75	72	c	c	c
93	71	72	c	c	c
70	56	75	c	c	c
51	35	59	p	c	c
62	50	55	c	c	c
67	77	55	c	c	c
71	56	53	c	c	c
50	29	42	c	c	c
44	38	24	p	c	c
33	27	37	c	c	c
41	54	34	p	p	p
51	61	40	c	p	p
38	30	39	p	p	p

p - partial; c - complete

Chapter IV

Experimental Procedure

4.1 Materials and Their Preparation

The chemical composition of the steel used in the present investigation is given in Table 4.1.

Table 4.1

Composition of the steel used

Alloy designation	Weight percentage of elements					
	C	Mn	Nb	V	P	S
C	0.20	1.24	0.0	0.0	0.011	0.004
Nb-V	0.18	1.35	0.034	0.03	0.005	0.008

The steels, supplied by STELTECH, Hamilton, Canada, were in the form of plates (transfer bars) about 5 cm in thickness and 1 m x 1 m in size. Blocks of sizes 18 cm x 12 cm x 5 cm were cut out from the plates and soaked for 2 hours at 1250°C in an electric muffle furnace. Some of the plates were also soaked for 2 hours at 1150°C. Controlled rolling (upto 90% reduction in thickness) was carried out in a reversing mill at CANMET, Ottawa. The rolling schedule was so chosen that in each case the rolling started at around 1200°C. For each steel, four samples were controlled rolled and finished - one at 1020°C (recrystallized range) after 5 passes, the second one at 850°C

(unrecrystallized range) after 6 passes, the third one at 730°C (γ+α range) after 6 passes and the fourth one at 630°C (α range) after 7 passes . While in the first sample the total amount of 90% deformation was given in the recrystallized range, in the subsequent samples about 70% of the total deformation was given in the previous ranges and the remaining 20% was given in the finishing range.

The temperature during controlled rolling was closely monitored by using thermocouples drilled into a hole in the central part of a number of trial samples from each steel. Optical pyrometers placed above the surfaces of the rolled material were calibrated against the thermocouple readings from the centres of the samples. This calibration chart was subsequently used to monitor the temperature of the samples during the actual controlled rolling operation. After the rolling operation all the samples were air-cooled to room temperature. A few were quenched immediately into agitated water in a bath.

4.2 Optical Metallography

4.2.1 Specimen Preparation and Examination

To study the optical microstructures of the different steel samples listed in Table 4.2, longitudinal sections of small metallographic samples were properly ground and subsequently polished in the usual manner. Each sample was prepared with repeated polishing and etching treatments using nital to produce a scratch-free microstructure showing reasonably good contrast. This etching treatment revealed the sizes and shapes

Table 4.2

Controlled rolled steel samples studied

		Steel No.	Comp. of steel	Def.	Finishing temperature	Aust. temperature
γ-RECRYST-ALLIZED	*1.	1RC	C	90%	1020°C	1250°C
	*2.	1RN	Nb-V	90%	1020°C	1250°C
	*3.	2RNQ	Nb-V	90%	1020°C(Qd.)	1250°C
	4.	3RC	C	75%	1020°C	1250°C
	5.	3RN	Nb-V	75%	1020°C	1250°C
	6.	4RCQ	C	75%	1020°C(Qd.)	1250°C
	7.	4RNQ	Nb-V	75%	1020°C(Qd.)	1250°C
γ-UNRECRY-STALLIZED	*8.	1N	Nb-V	90%	850°C	1250°C
	*9	2NQ	Nb-V	90%	850°C(Qd.)	1250°C
	*10.	3C	C	75%	850°C	1250°C
	11.	3N	Nb-V	75%	850°C	1250°C
	12.	4NQ	Nb-V	75%	850°C(Qd.)	1250°C
γ+ α-RANGE	*13.	1TC	C	90%	730°C	1250°C
	*14.	1TN	Nb-V	90%	730°C	1250°C
	15.	2TC	C	75%	730°C	1250°C
	16.	2TN	Nb-V	75%	730°C	1250°C
	17.	1TCA	C	90%	770°C	1250°C
	18.	1TNA	Nb-V	90%	770°C	1250°C
	19.	2TCA	C	75%	770°C	1250°C
	20.	2TNA	Nb-V	75%	770°C	1250°C
α-RANGE	*21.	1FC	C	90%	630°C	1250°C
	*22.	1FN	Nb-V	90%	630°C	1250°C
	23.	2FC	C	75%	630°C	1250°C
	24.	2FN	Nb-V	75%	630°C	1250°C
γ-RECRYS-TALLIZED	25.	L1RC	C	90%	1020°C	1150°C
	26.	L1RN	Nb-V	90%	1020°C	1150°C
	27.	L2RCQ	C	90%	1020°C(Qd.)	1150°C
	28.	L2RNQ	Nb-V	90%	1020°C(Qd.)	1150°C

Continued...

	Steel No.	Comp. of steel	Def.	Finishing temperature	Aust. temperature
γ-UNRECR-YSTALLIZED					
29.	L1C	C	90%	850°C	1150°C
30.	L1N	Nb–V	90%	850°C	1150°C
31.	L2CQ	C	90%	850°C(Qd.)	1150°C
32.	L2NQ	Nb–V	90%	850°C(Qd.)	1150°C
α + γ RANGE					
33.	L1TC	C	90%	730°C	1150°C
34.	L1TN	Nb–V	90%	730°C	1150°C
35.	1TCAL	C	90%	770°C	1150°C
36.	1NTAL	Nb–V	90%	770°C	1150°C
α-RANGE					
37.	L1FC	C	90%	630°C	1150°C
38.	L1FN	Nb–V	90%	630°C	1150°C

* These samples were studied in detail.

of the pearlite and martensite properly and could also deli-
neate the ferrite regions satisfactorily. With this etching
treatment the martensitic needles and pearlite islands were
etched dark while the ferrite matrix was etched bright. After
etching, the specimens were washed in running water, rinsed
with methanol and dried. Photomicrographs were taken from
these etched surfaces using Lietz Metallux 3 optical microscope
at magnifications 200X, 500X and 1000X.

4.3 Quantitative Metallography

4.3.1 Grain Size Distribution Using Intercept Method

The grain-sizes of ferrite in the controlled rolled
steels were measured in an optical microscope using the
intercept method. The principle of this method involves
counting the number of grains intercepted by a theoretical line
on the specimen surface. The grain size was calculated by
dividing the length of the line by the product of the number
of intercepts along that line of the ferrite grains and the
concerned magnification. An average of about six such measu-
rements of grain sizes was taken for each sample to get the
final average grain size. For anisotropic grains calculations
were made for the average length and width of the grains
separately by taking the intercepts both along the length of
the grain and its perpendicular direction.

4.3.2 Grain Size Distribution Measurement Using Image Analyser

An Omnicon Alpha 500 Image Analyser was also used to determine the grain size distribution of the ferrite of a few samples. The grain size distribution was noted at five random locations on the surface of each sample and the values obtained were then averaged out. Histograms were plotted to record the percentage of particles over different pre-determined size ranges.

4.4 Transmission Electron Microscopy

Slices having an area of 25 mm x 25 mm and a thickness of 0.5 mm were cut using a Buehler Isomet diamond cutting saw, from the longitudinal sections of all the different steel samples.

All the slices were first mechanically thinned down to a thickness of 0.06 mm by polishing on moistened emery papers. To start with, these mechanically thinned down specimens were first cleaned with acetone and then 3 mm discs were punched out from these mechanically thinned and cleaned samples with the help of a die and punch.

Final electropolishing of the discs was carried out to produce a thinned central region supported by a thicker outside rim using a jet polishing device (Tenupol unit). For this purpose, an electrolyte containing 10 volume % perchloric acid in glacial acetic acid was used at a temperature of $<10^{o}C$ and at a potential difference of 40 volts. The thinned perforated foils were rinsed with running water, then with ethyl alcohol and finally dried. Transmission electron microscopy

of the thin foils was carried out on a Philips EM301 machine operated at 100 kV and also on a JEM 2000 FX operated at 120 kV.

All the T.E.M. work was carried out on thin foils made from the longitudinal sections of the rolled sheets. S.A.D. patterns were taken from selected number of specimens.

4.5 Determination of Texture

Crystallographic textures were determined from the mid-sections of the samples listed in Table 4.2. Specimens of size 25 mm x 14 mm were cut out from sheets of the different materials. The dimension along the rolling direction is 25 mm and that along the transverse direction is 14 mm.

In all texture specimens, a little less than half of the total thickness was removed from one of the flat surfaces by milling. The specimens were then ground and polished metallographically and then etched lightly to remove any disturbed layer. The {200} pole-figures were determined from these texture samples by the Schulz reflection method [113] using CoK_α radiation with an iron filter. Intensity levels on the pole-figures were determined by comparison with the intensity obtained from a solid specimen of pure iron which had been randomised by repeated deformation and annealing.

Chapter V

Results and Discussion

5.1 Textures in Plain C and Nb-V Steels

The (200) pole-figures for the plain C steel finish rolled at the four different temperatures are shown in Figures 5.1 - 5.4. Figures 5.1 - 5.3 are not much different from one another; all are rather weak in intensity and show quite similar pole distribution. The orientations present in all the three are {100} <011>, {113} < 110> and {332} <113> $\sim$ {554} <225>. A slightly sharper texture is obtained after ferrite rolling (Figure 5.4). Here the texture components appear as {100} <011>, {554} <225> and {112} <110> $\sim$ {113} <110>.

The (200) pole-figures for the Nb-V steel finish rolled at the four different temperatures are presented in Figures 5.5 - 5.8. A comparison between these pole-figures and the one for the plain C steel clearly shows that the former are perceptibly more intense than the latter. Although the pole distribution pattern in Figures 5.1 and 5.5 are quite similar, the situation is quite different for Figures 5.2 and 5.3 on the one hand and Figures 5.6 and 5.7 on the other. The main orientations present in the textures of the Nb-V steel, finish rolled at $850^{\circ}C$ and $730^{\circ}C$ are {100} <011> and {112} <110> $\sim$ {113} <110>. The texture of the Nb-V steel after ferrite rolling (Figure 5.8) is almost identical with the texture of similarly treated plain C steel.

^ {112}<110>

Fig. 5.1

Plain C / Tf = 1020 °C
Contour Levels:
1.00, 1.10, 1.20, 1.30, 1.40, 1.50, 1.60

Fig. 5.2

Plain C / Tf = 850 °C
Contour Levels:
1.00, 1.10, 1.20, 1.30, 1.40, 1.50, 1.60

Fig. 5.3

Plain C / Tf = 730 °C
Contour Levels:
1.00, 1.15, 1.30, 1.45, 1.60, 1.75, 1.90

Fig. 5.4

Plain C / Tf = 630 °C
Contour Levels:
1.00, 1.20, 1.40, 1.60, 1.80, 2.00, 2.20

(200) Pole Figures
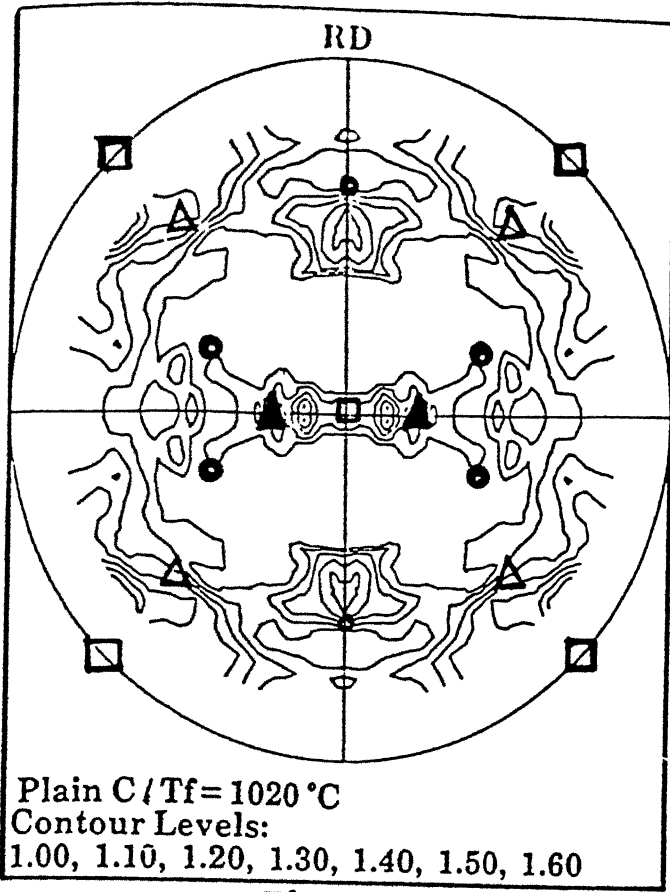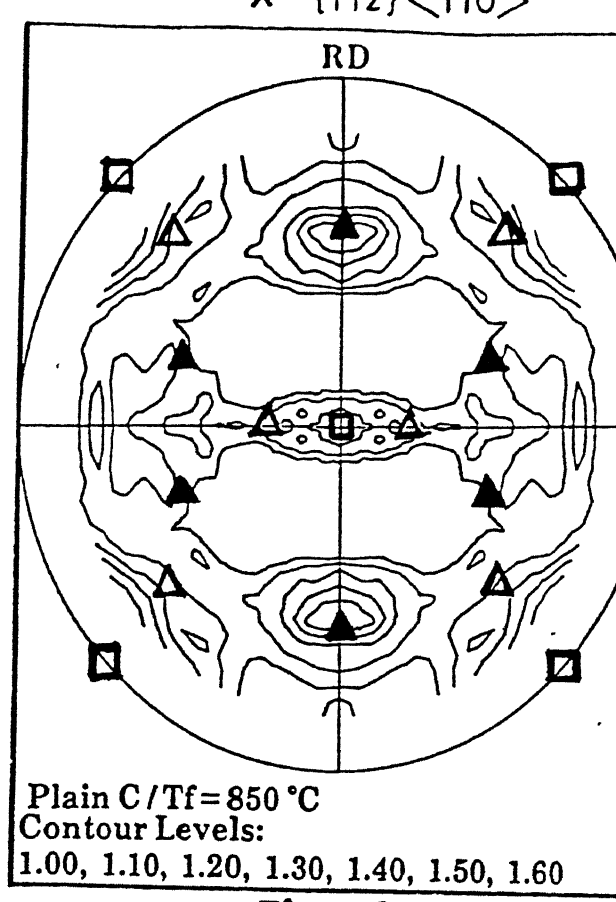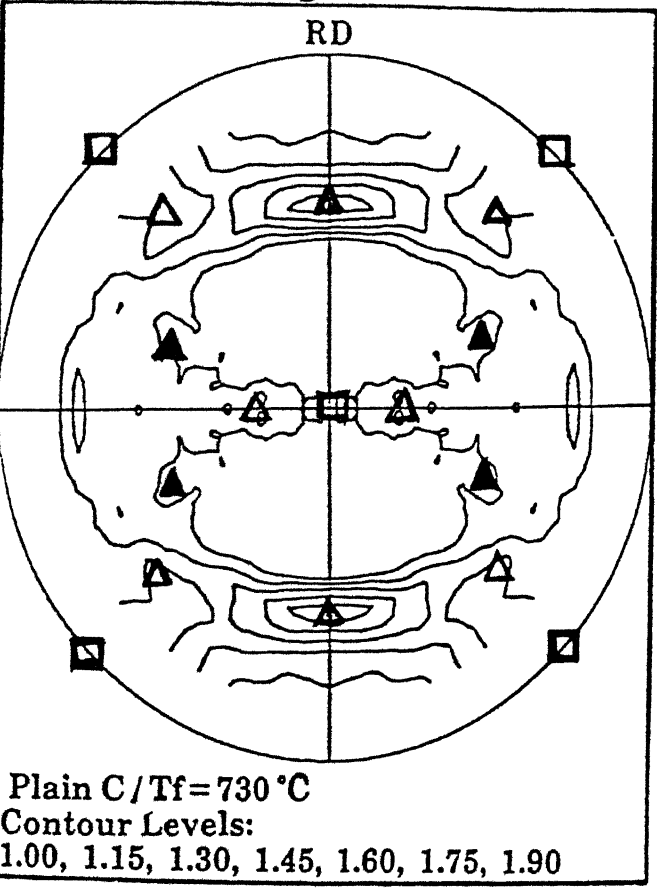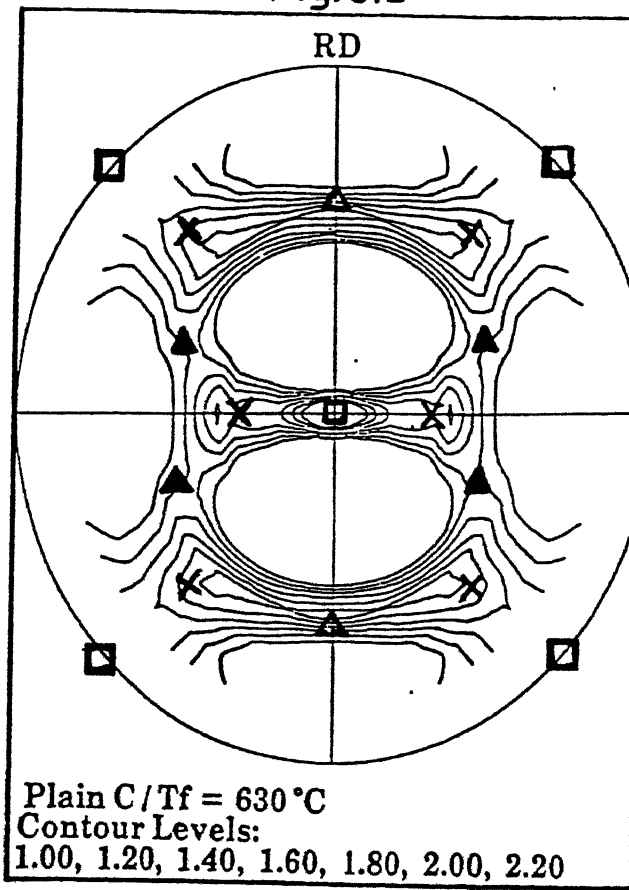
It is clearly understood that the textures obtained from the materials finish rolled at $1020^{o}C$ (within γ recrystallization range) and $850^{o}C$ (within γ non-recrystallization range) are basically the transformation textures. These are obtained due to the formation of recrystallization and 'cold-worked' textures in the worked γ, which are subsequently transformed into the corresponding ferrite textures during cooling. It is known that (Ray and Jonas's paper [23]) the major texture component of recrystallized γ is the cube texture, $\{100\} <001>$, which gets transformed into the $\{100\} <011>$ component after the $\gamma \rightarrow \alpha$ phase transformation. The two major components of the texture of unrecrystallized γ are $\{110\} <112>$ and $\{112\} <111>$ which transform into $\{332\} <113>$ and $\{113\} <110>$ respectively in the transformed ferrite.

All the three transformation texture components (obtained from both recrystallized and unrecrystallized γ) could be noticed in the pole-figures of the plain C steel finish rolled at $1020^{o}C$, $850^{o}C$ and $730^{o}C$ (Figures 5.1 - 5.3). Of course, these texture components are very weak indeed in all the three pole-figures. It has to be remembered that these samples were first rolled in the recrystallized γ region - one sample was finished ($1020^{o}C$) in that region only; the second one was further rolled in the γ non-recrystallization region and finished ($850^{o}C$) in that region, whereas the third sample was progressively rolled in the ($\gamma + \alpha$) region and finished ($730^{o}C$), in that region only. Naturally both the samples finished at $850^{o}C$ and $730^{o}C$ are expected to contain

not only the transformed γ unrecrystallized components, but also the transformed γ recrystallization component. Since the intensity levels of the texture components are rather low in both the cases, it is not possible to dwell on the relative strengths of the components from one sample to the other. The presence of the transformed γ-unrecrystallized components in the 1020°C finished material is rather surprising. This should contain only the transformed γ-recrystallization component, which is {100} <011>. The presence of the former components in this sample may indicate the possibility that these are derived as remnants of the texture that might have been present in the original transfer bar.

The components {100} <011>, {113} <110> and {332} <113> are also found to constitute the transformation texture of the 1020°C finished Nb-V steel. The origin of these components in this sample can be accounted in the same manner as assumed for the corresponding plain C steel. However, there is a noticeable change in the nature and intensity of the overall texture for the 850°C and 730°C finished samples of the Nb-V steel when compared to the corresponding plain C steel. The former are somewhat different and distinctly more sharp as compared to the latter. For example, the {112} <110> ~ {113} <110> component is more than twice as sharp in the Nb-V steel as compared to the plain C steel. The relatively higher intensities of the transformation texture components derived from unrecrystallized γ over that derived from recrystallized γ in the Nb-V steel, clearly indicates that γ recrystallization is effectively retarded in this steel. Many investigators [17,

18, 47-60] have suggested that Nb has a strong retarding effect on ~ recrystallization. This has been attributed to:

(a) the strain-induced precipitation of fine Nb(C,N) part-icles and

(b) a combination of solute drag and precipitation effects. Obviously a similar phenomenon is occurring in the present Nb-V steel also which effectively gives rise to a much shaper texture.

There is practically no difference in the textures of samples finish-rolled at $630^{\circ}C$ for both the plain C and the Nb-V steels. This is hardly unusual since here the most prominent part in texture formation is played by ferrite rolling. Here the effect of transformation texture is expected to be much less since such components formed at higher temper-atures will be effectively modified and intensified by the ferrite rolling carried out at a comparatively low temperature.

5.2 Optical Microstructures

Figures 5.9 - 5.19 show the optical micrographs of the two steels finish rolled at different temperatures. Figures 5.9 and 5.10 show the microstructures obtained for the plain C and the Nb-V steel respectively finished rolled at $1020^{\circ}C$ (γ-recrystallization range). The ferrite phase in both appear to have fully recrystallized. However, whereas the pearlite appears mostly as rather equiaxed grains in the plain C steel, the pearlitic areas appear as deformed and elongated stringers in the Nb-V steel. The microstructures of the samples quenched from the finish rolling temperature of $1020^{\circ}C$ consist

essentially or martensite, shown typically for the Nb-V steel, in Figure 5.11. A higher magnification micrograph (Figure 5.12) shows that the martensite here exhibits a typical "packet" morphology.

Although the microstructure of the plain C steel finish rolled at 850°C shows essentially recrystallized grains of ferrite and pearlite (Figure 5.13), the corresponding microstructure for the Nb-V steel shows both recrystallized and unrecrystallized ferrite grains (Figure 5.14). The recrystallized grains have a mixed grain size, while the unrecrystallized/partially recrystallized grains appear elongated along the rolling direction. The pearlite here appears deformed and elongated. The quenched samples of both the steels at this stage consist essentially of martensite and these are obtained as bands, obviously elongated along the rolling direction. This is shown typically for the Nb-V steel in Figure 5.15.

Figures 5.16 and 5.17 show the optical microstructures of the plain C and the Nb-V steel respectively, after finish rolling at 730°C (α + γ intercritical range). While the microstructure of the plain C steel shows a larger volume fraction of almost equal sized recrystallized ferrite grains and only a small volume fraction of unrecrystallized or partially recrystallized grains, the situation is quite different for the Nb-V steel. Here the number of unrecrystallized or partially recrystallized ferrite grains are more profuse than in the corresponding plain C steel sample. Moreover, the
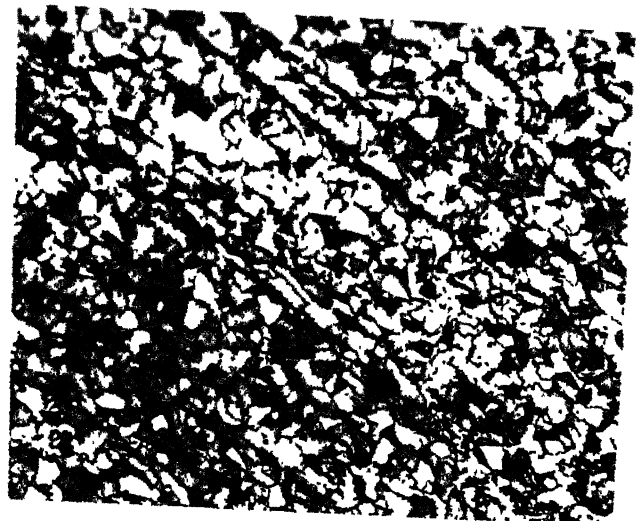
FIGURE 5.9
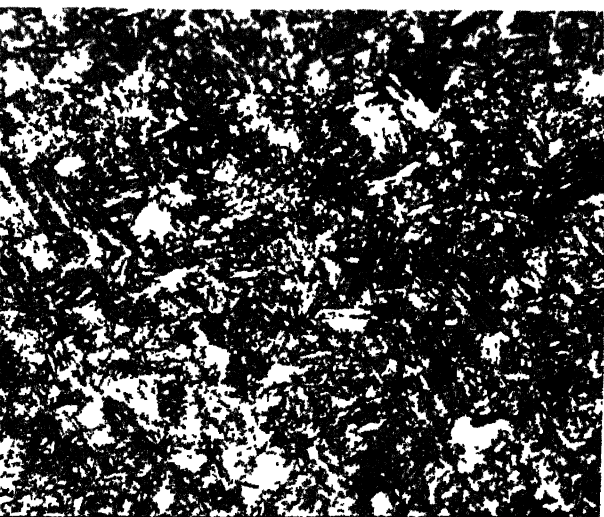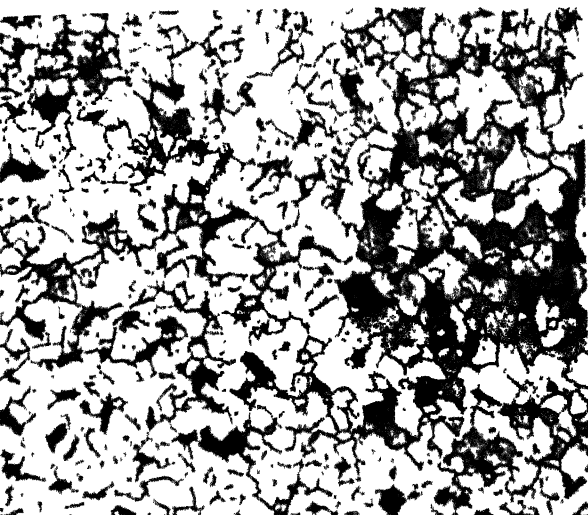(M = 200X)

FIGURE 5.10
(M = 200X)

FIGURE 5.11
(M = 200X)

FIGURE 5.12
(M = 1000X)

Figures 5.9-5.12   Optical microstructures of materials with
                    austenitizing temperature 1250°C and finish
                    rolling temperature 1020°C.

Figure 5.9   C-steel aircooled after 90% deformation (1RC).

Figure 5.10   Nb-V steel aircooled after 90% deformation (1RN).

Figures 5.11   Nb-V steel water quenched after 90% deformation
-5.12   (2RNO).

FIGURE 5.13
(M=200X)

FIGURE 5.14
(M=500X)

FIGURE 5.15
(M=1000X)

Figures 5.13-5.15   Optical microstructures of materials with
austenitizing temperature 1250°C and finish
rolling temperature 850°C.

Figure 5.13   C-steel air cooled after 75% deformation (3C).

Figure 5.14   Nb-V steel air cooled after 90% deformation (1N).

Figure 5.15   Nb-V steel water quenched after 90% deformation
(2NQ).

ferrite grains are of mixed size - some are quite fine as compared to the others. The pearlite in both, Figures 5.16 and 5.17, appear deformed and elongated along the rolling direction.

The optical microstructures of the plain C and the Nb-V steels, finish rolled in the ferrite region (630°C), are shown in Figures 5.18 and 5.19 respectively. The ferrite grains, in both the figures appear deformed and elongated along the rolling direction. However, the dimensions of the deformed ferrite grains along the transverse direction are much finer for the Nb-V steel as compared to the plain C steel. The pearlitic regions in both the steels are deformed and elongated along the rolling direction.

The results of optical microscopy show that structurally there is hardly any difference between the plain C and the Nb-V steel finish rolled at 1020°C (γ-recrystallization range). However, sharp differences in the microstructures appear for the samples finish-rolled at 850°C (γ non-recrystallization range). Whereas the optical microstructure of the plain carbon steel at this stage clearly indicates considerable recrystallization, the corresponding microstructure for the Nb-V steel appears highly deformed. These differences persist for the samples finish rolled at 730°C (γ + α intercritical range). Finally, after ferrite rolling (at 630°C) the microstructural features for both the plain C and the Nb-V steel appear to be quite similar.

The variation of the microstructural features for the two steels, as a function of the finish rolling temperature,
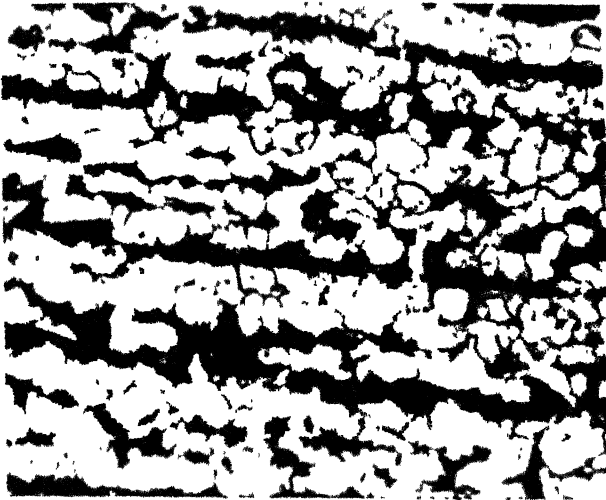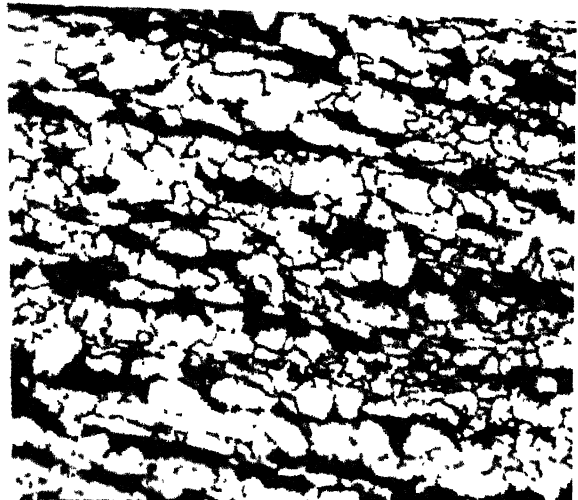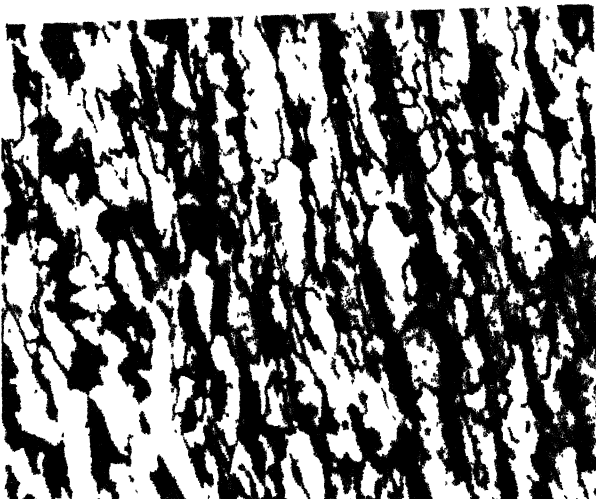
FIGURE 5·16
(M = 500X)

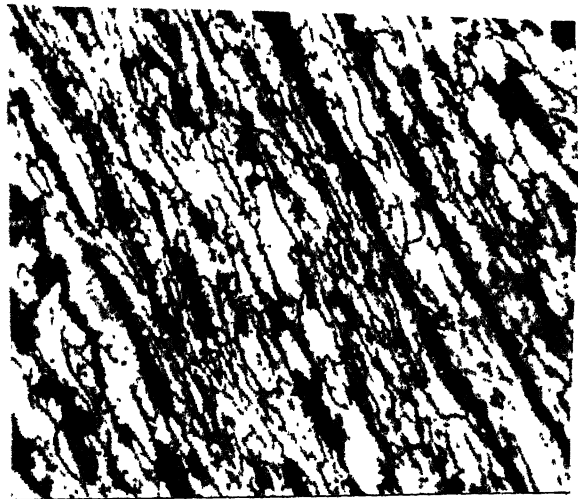FIGURE 5·17
(M = 500X)

FIGURE 5·18
(M = 500X)

FIGURE 5·19
(M = 500X)

Figures 5.16–5.19   Optical microstructures of materials with austenitizing temperature 1250°C.

Figure 5.16   C-steel air cooled after 90% deformation finish rolled at 730°C (1TC).

Figure 5.17   Nb-V steel air cooled after 90% deformation fini rolled at 730°C (1TN).

Figure 5.18   C-steel air cooled after 90% deformation finish rolled at 630°C (1FC).

Figure 5.19   Nb-V steel air cooled after 90% deformation finish rolled at 630°C (1FN).

is also reflected in the variation of the crystallographic textures for the corresponding samples, as mentioned previously. Thus, the textures of the 1020°C finished samples of both the plain C and the Nb-V steels are found to be quite similar. On the other hand, the overall textures of the 850°C and 730°C finished samples of the Nb-V steel are found to be much sharper as compared to those of the corresponding samples of the plain C steel. In fact, in the textures of the Nb-V steel, the transformed components obtained from unrecrystallized γ are found to be much stronger in intensity than the component obtained from recrystallized γ. This is in stark contrast to the samples of the plain C steel similarly treated. The textural difference between the two steels is clearly reflected in the corresponding microstructures - the Nb-V steel showing more of ferrite obtained from deformed γ while the plain C steel shows a large volume fraction of ferrite obtained essentially from recrystallized γ. Finally, ferrite rolling produces similar texture in both the steels, which also show similar microstructure at this stage.

5.3 Grain-size Measurements

The results of the ferrite grain-size measurement for the different samples in both the steels are tabulated in Tables 5.1 and 5.2. For the nearly equiaxed grains, an average grain diameter was calculated, whereas for the elongated grains, averages of two of the major dimensions were measured (along the length and breadth of the grains). The ferrite

grain-size distributions for a few samples are given in Figures 5.20 - 5.23. The results are in general agreement with those shown in Tables 5.1 and 5.2.

The major findings of the grain-size measurement results can be stated as follows:

a) For any steel there is, in general, a progressive decrease in the ferrite grain-size, as the finishing temperature of rolling decreases.

b) In general, for any steel, for any finishing temperature, the ferrite grain-size decreases as the total amount of deformation by rolling increases.

c) In any steel, other variables remaining constant, a lower austenitising temperature produces a smaller ferrite grain-size after controlled rolling.

d) For the same austenitising temperature, similar amounts of rolling reduction and same finishing temperature, much finer ferrite grain-size is produced in the Nb-V steel as compared to the plain C steel.

Overall, the grain-size measurements indicate that controlled rolling at progressively lower temperatures, starting from the γ recrystallization range and finishing in the ferrite range, produces the finest ferrite grain size. The Nb-V steel definitely has an edge over the plain C steel in this respect.

5.4 Electron Microstructures

Figures 5.24 - 5.49 show a series of transmission electron microstructures taken from a number of samples of

Table 5.1

Grain size measurement results

Austenitizing Temperature = 1250°C

	Sample designation	C or Nb-V	Amount of deformation	Finishing temp. (^{O}C)	Grain size (X 10^{-3} cm)
γ-RECRYST-ALLIZED	1RC	C	90%	1020	4.83
	1RN	Nb-V	90%	1020	2.006
	3RC	C	75%	1020	3.227
	3RN	Nb-V	75%	1020	1.22
γ-UNRECRYS-TALLIZED	1N	Nb-V	90%	850	1.482 (R.D.) 1.121 (T.D.)
	3C	C	75%	850	1.421
	3N	Nb-V	75%	850	1.239
$\gamma + \alpha$ RANGE	1TC	C	90%	730	0.873 (R.D.) 0.838 (T.D.)
	1TN	Nb-V	90%	730	0.955 (R.D.) 0.656 (T.D.)
	2TC	C	75%	730	1.251
	2TN	Nb-V	75%	730	0.536
	1TCA	C	90%	770	0.676 (R.D.) 0.671 (T.D.)
	1TNA	Nb-V	90%	770	0.690 (R.D.) 0.546 (T.D.)
	2TCA	C	75%	770	0.935
	2TNA	Nb-V	75%	770	0.844
α RANGE	1FC	C	90%	630	0.992 (R.D.) 0.638 (T.D.)
	1FN	Nb-V	90%	630	2.179 (R.D.) 0.670 (T.D.)
	2FC	C	75%	630	0.955
	2FN	Nb-V	75%	630	1.188

Table 5.2

Grain size measurement results

Austenitizing Temperature = 1150°C

	Sample designation	C or Nb-V	Amount of deformation	Finishing temp. (^{O}C)	Grain size (X 10^{-3} cm)
γ-RECRYST-ALLIZED	L1RC	C	90%	1020	1.437 (R.D.) 1.094 (T.D.)
	L1RN	Nb-V	90%	1020	1.104
γ-UNRECRYST-ALLIZED	L1C	C	90%	850	1.771 (R.D.) 1.176 (T.D.)
	L1N	Nb-V	90%	850	0.733 (R.D.) 0.741 (T.D.)
α + γ RANGE	L1TC	C	90%	730	1.076 (R.D.) 0.7013(T.D.)
	L1TN	Nb-V	90%	730	1.216 (R.D.) 0.621 (T.D.)
	1TCAL	C	90%	770	1.006 (R.D.) 0.907 (T.D.)
	1NTAL	Nb-V	90%	770	0.772 (R.D.) 0.556 (T.D.)
α RANGE	L1FC	C	90%	630	1.946 (R.D.) 0.812 (T.D.)
	L1FN	Nb-V	90%	630	1.797 (R.D.) 0.568 (T.D.)
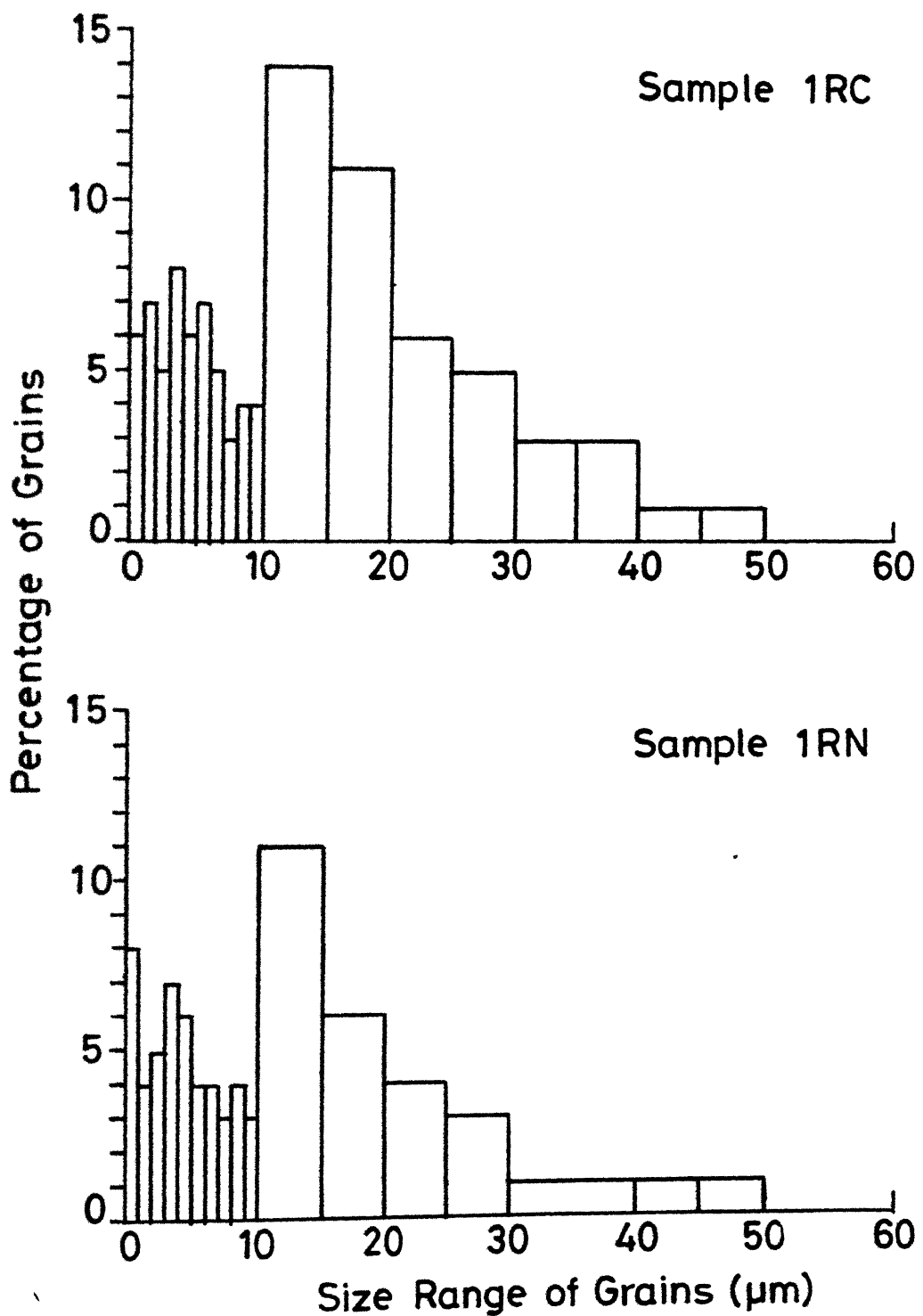
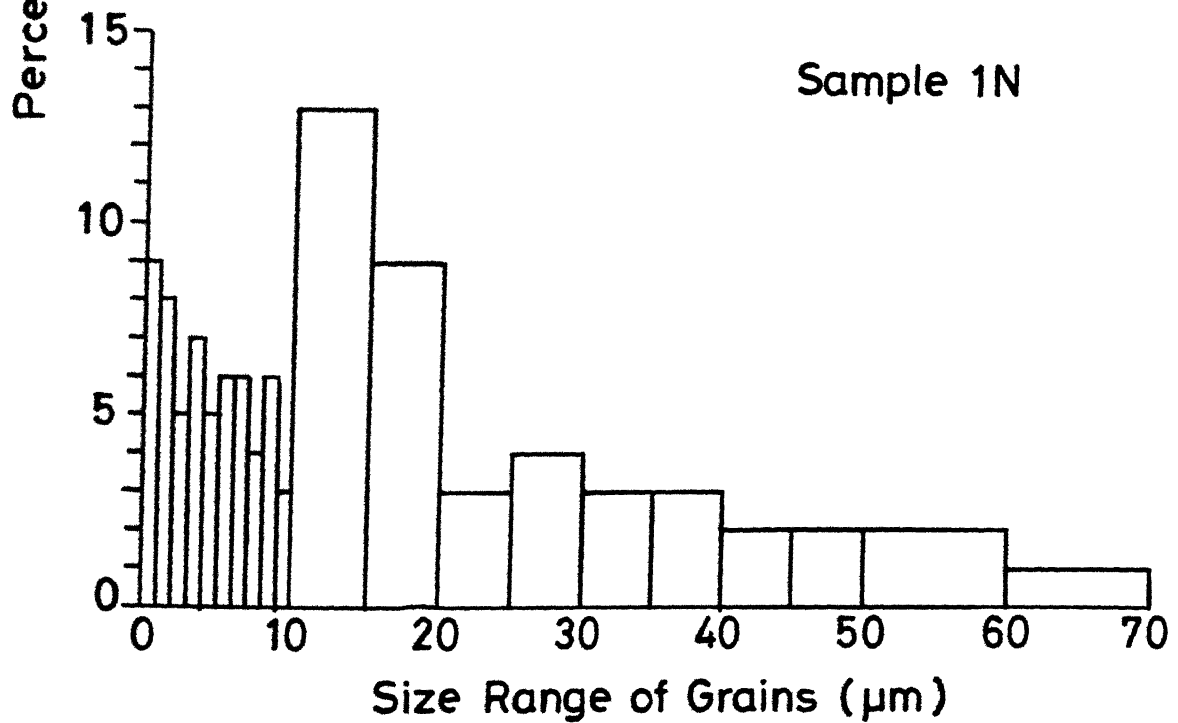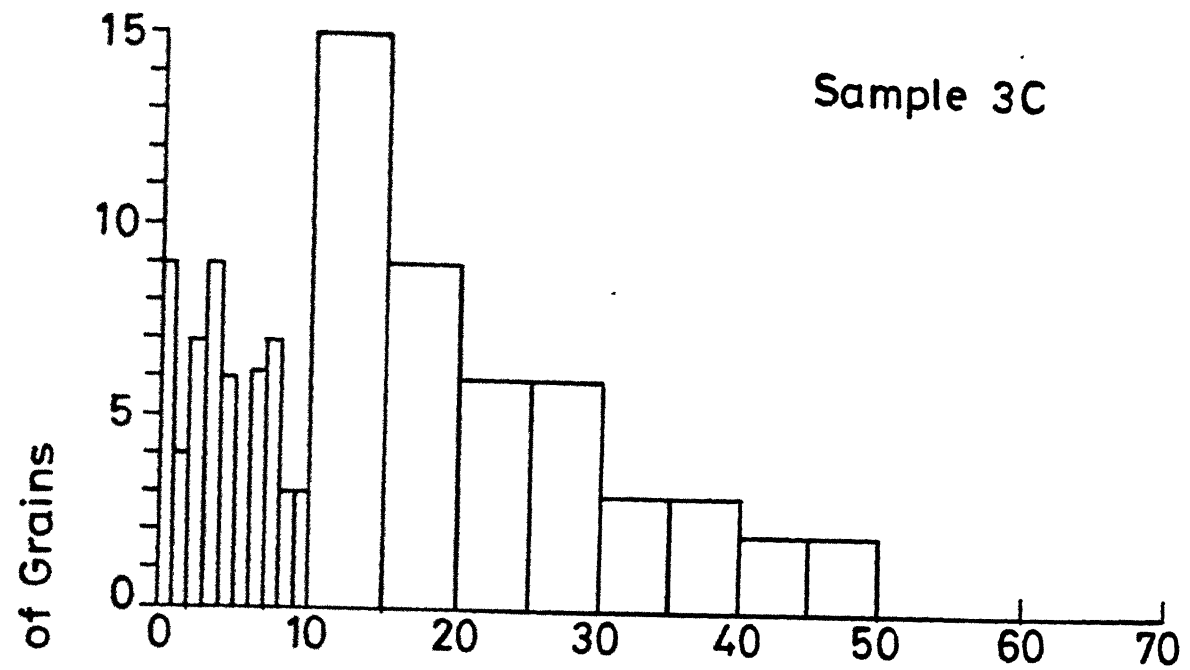Fig.5.20 Grain size distribution in controlled rolled
steel.

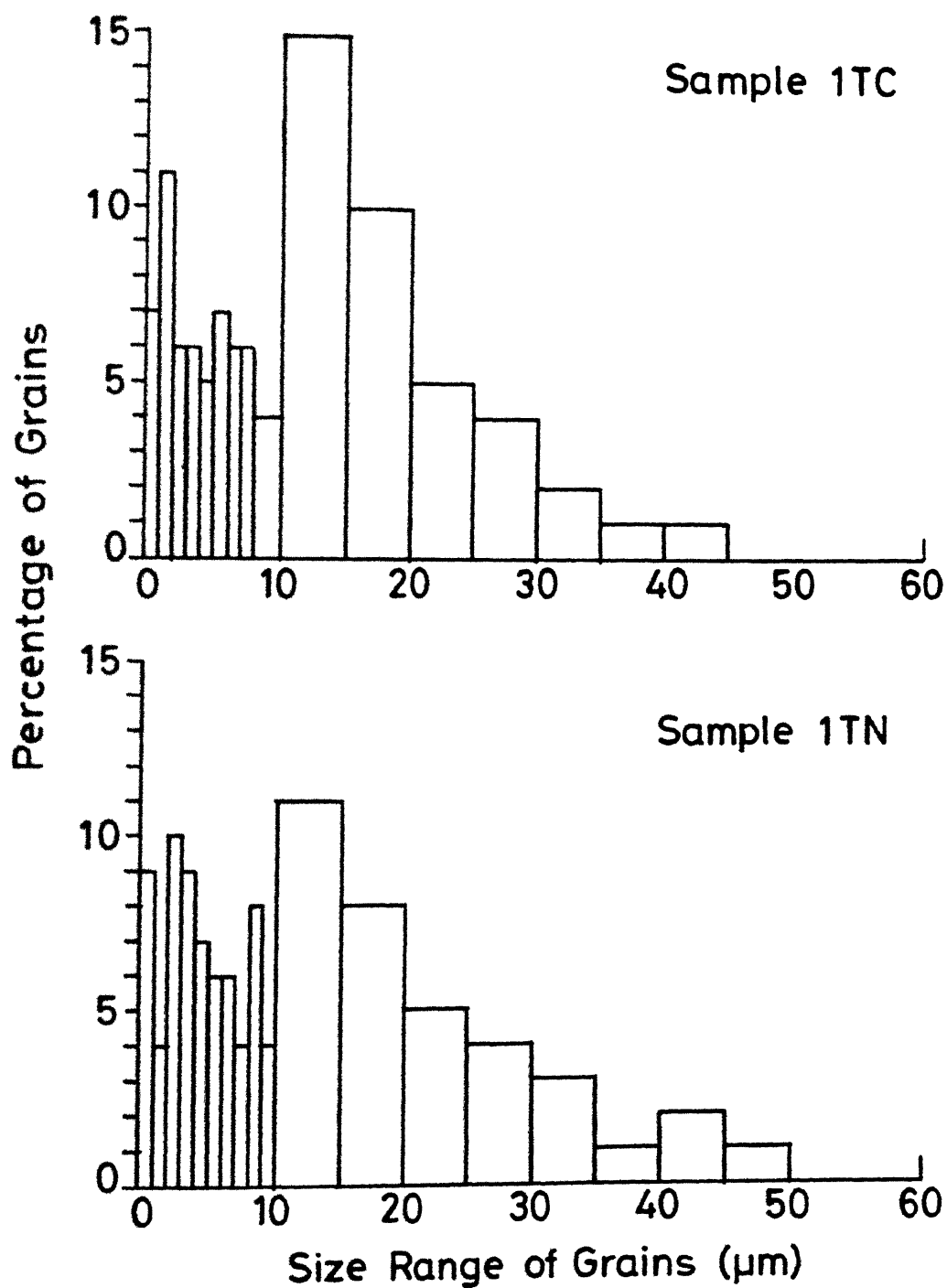Fig. 5.21 Grain size distribution in controlled rolled steel.

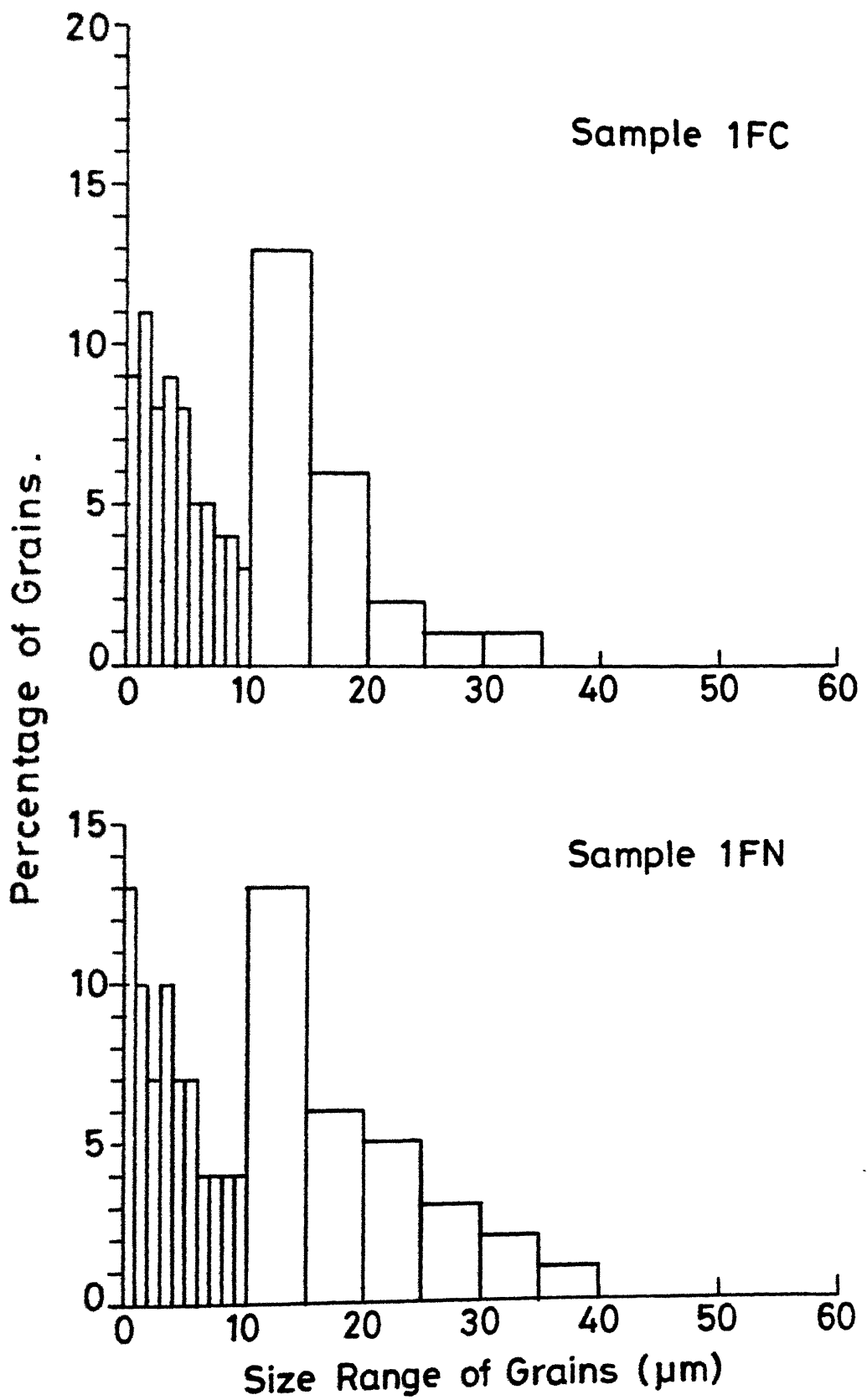Fig. 5.22 Grain size distribution in controlled rolled steel.

Fig. 5.23 Grain size distribution in controlled rolled steel.

both the steels, finished at different temperatures. Figure 5.24 shows the TEM of the plain C steel finish rolled at 1020°C. The microstructure shows a ferrite grain and a pearlitic area side by side. The ferrite grain seems to possess a substructure. At a higher magnification this substructure could be resolved as some fine particles which are dislocation-nucleated at many places (Figure 5.25). The identity of these particles could not be determined by selected area diffraction (SAD). A general view of the microstructure obtained for the Nb-V steel, finish rolled at 1020°C, is given in Figure 5.26. The structure consists essentially of ferrite grains (from recrystallized γ) and pearlite. Figure 5.27 shows another area at a higher magnification that reveals fine lamellar structure of the pearlite. The ferrite grains are found to contain a large number of dislocation-nucleated particles (Figure 5.28). The SAD from this area is presented in Figure 5.29 and this could be indexed as for the b.c.c. (110) plane. However, from the observed pattern the precipitate particles could not be identified.

A typical ferrite-pearlite microstructure for the plain C steel finish rolled at 850°C is shown in Figure 5.30. The ferrite grains are large and sometimes show a dislocation substructure inside (Figure 5.31).

Figure 5.32 shows the electron microstructure of the Nb-V steel finish rolled at 850°C. The structure here consists of ferrite grains, some much finer than the others, together with pearlitic areas. A magnified image of another
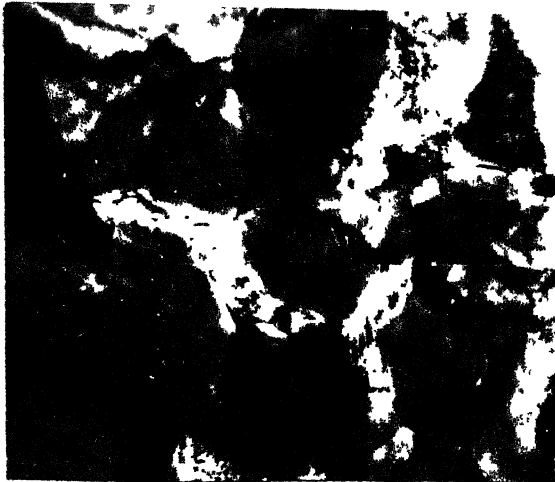
FIGURE 5.24 (M = 30k)

FIGURE 5.25 (M = 80k)

FIGURE 5.26 (M = 5k)

FIGURE 5.27 (M = 10k)

FIGURE 5.28 (M = 30k)

FIGURE 5.29 (CL = 80(w)

Figures 5.24–5.29	Transmission electron micrographs of materials with austenitizing temperature 1250°C and finish rolling temperature 1020°C.
Figures 5.24–5.25	C-steel air cooled after 90% deformation
Figures 5.26–5.29	Nb-V steel air cooled after 90% deformation (1RN).

region (Figure 5.33) shows a pearlitic area at a triple point. There are some isolated dislocation in neighbouring ferrite grains.

A microstructure consisting essentially of fine ferrite grains and pearlite (Figure 5.34) is obtained for the plain C steel finish rolled at 730°C. A similar microstructure has been found for the Nb-V steel finish rolled at the same temperature (Figure 5.35). The ferrite grains here occasionally show a dislocation network inside (Figure 5.36).

The electron microstructures of both the steels after ferrite rolling (finished at 630°C) appear to be distinctly different from the structures described above. Figure 5.37 shows a general view of the microstructure obtained for the plain C steel at this stage. The structure consists essentially of highly deformed and dislocated ferrite grains. Isolated pearlite colonies are also observed sometimes (Figure 5.38). Deformed ferrite grains of somewhat finer size are observed in the electron microstructure of the Nb-V steel finished rolled in the ferrite region (Figure 5.39). Even the pearlitic colonies are seen to undergo some amount of plastic deformation at this stage (Figure 5.40). Although the ferrite grains appear quite clean, SAD patterns from them sometime show extra spots. This is illustrated in Figures 5.41 and 5.42 which show a central ferrite grain and the SAD therefrom. The extra spots in the SAD are quite intense; however, no clear-cut precipitates or any other feature can
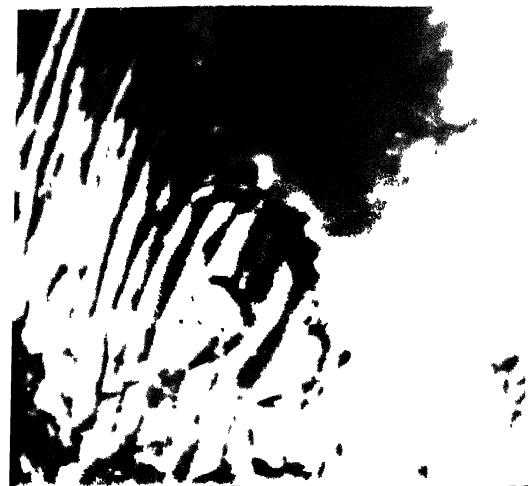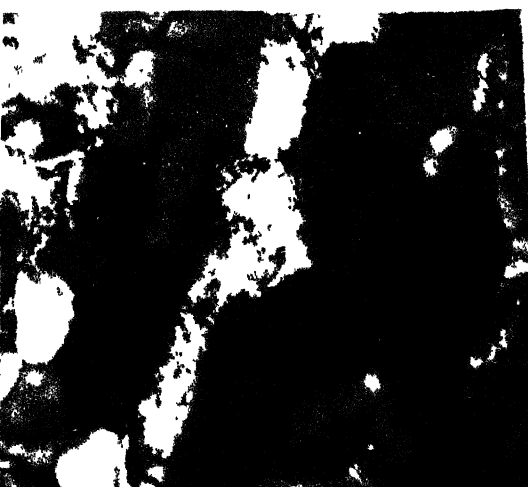
FIGURE 5·30
(M = 20K)

FIGURE 5·31
(M ≈ 6K)

FIGURE 5·32
(M = 4K)

FIGURE 5·33
(M = 10K)

Figures 5.30–5.33   Transmission electron micrographs of materials
                      with austenitizing temperature 1250°C and
                      finish rolling temperature 850°C

Figures 5.30–5.31   C-steel air cooled after 75% deformation (3C).

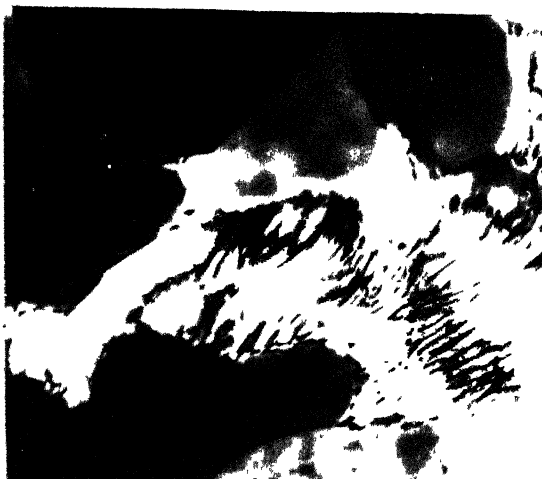Figures 5.32–5.33   Nb-V steel air cooled after 90% deformation

FIGURE 5.34
(M = 13K)

FIGURE 5.35
(M = 8K)

FIGURE 5.36
(M = 40K)

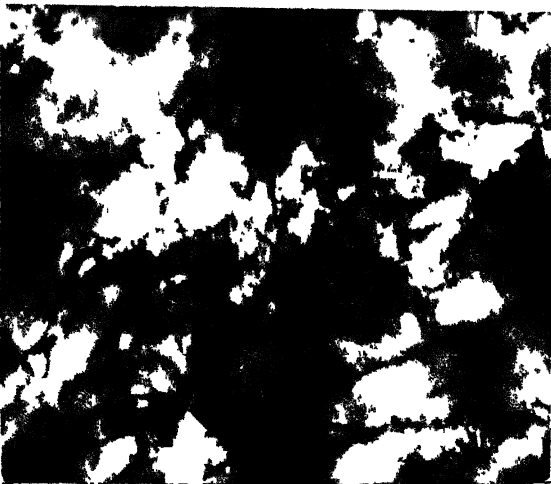| Figures 5.34-5.36	Transmission electron micrographs of materials with austenitizing temperature 1250°C and finish rolling temperature 730°C.
Figure 5.34	C-steel air cooled after 90% deformation (1TC).
Figures 5.35-5.36	Nb-V steel air cooled after 90% deformation (1TN).

FIGURE 5.37 (M=50k)

FIGURE 5.38 (M=30k)
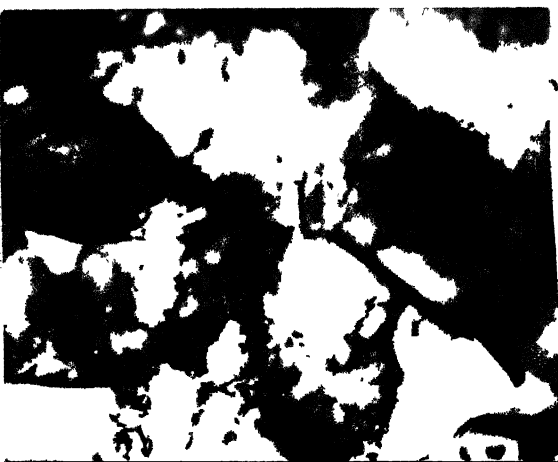

FIGURE 5.39 (M=10K)

FIGURE 5.40 (M=30K)

FIGURE 5.41 (M=80k)

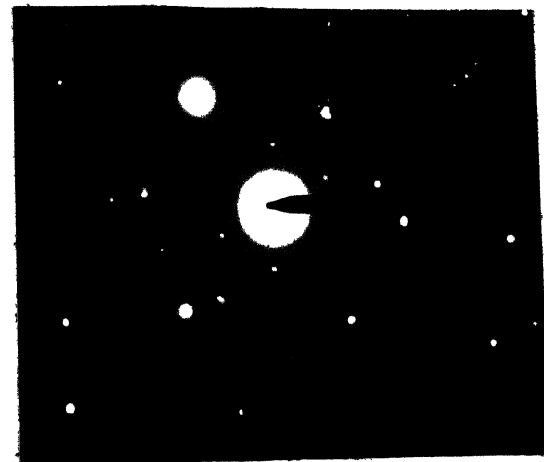FIGURE 5.42 (CL=80cm)

Figures 5.37-5.42   Transmission electron micrographs of materials with austenitizing temperature 1250°C and finish rolling temperature 630°C.

Figures 5.37-5.38   C-steel air cooled after 90% deformation (1FC)

Figures 5.39-5.42   Nb-V steel air cooled after 90% deformation (1FN).

be seen in the micrograph. The spots could not be indexed in terms of any expected phase or phases.

During the current investigation transmission electron micrographs were also taken from a few samples which were control rolled and subsequently quenched. Figure 5.43 shows a typical microstructure of the Nb-V steel finish rolled in the γ-recrystallization range (1020°C) and then immediately quenched in water. The structure essentially consists of martensite laths - typically showing the "packet" morphology. Sometimes thin regions containing lots of precipitate particles can be seen sandwiched between martensitic regions (Figure 5.44). A higher magnification micrograph (Figure 5.45) shows the precipitate morphology more clearly. In fact, the precipitate particles appear to be needle-shaped or platelet-shaped. However, the corresponding SAD pattern (Figure 5.46), which indicates the b.c.c. (111) plane, surprisingly does not show any extra spots.

Figure 5.47 shows the morphology of the martensite obtained by quenching the Nb-V steel after it was control-rolled and finished in the γ non-recrystallization range (850°C). In some regions areas with fine particles, some of them dislocation-nucleated are also seen (Figure 5.48). A micrograph at a much higher magnification is shown in Figure 5.49. It was not possible to identify the precipitate particles in this case also.

The transmission electron microscopy results indicate that there is practically no difference in the microstructures
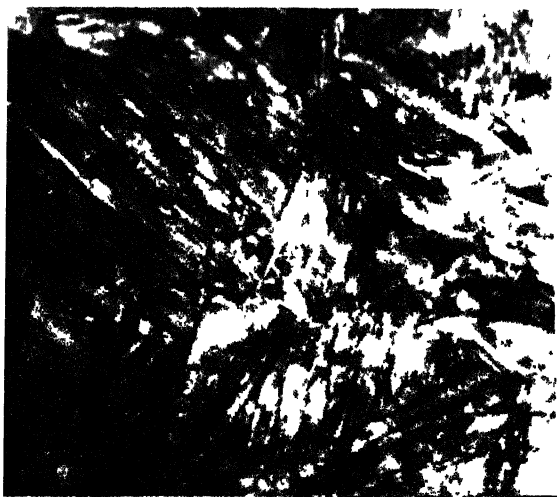
FIGURE 5.43
(M = 6K)

FIGURE 5.44
(M = 8K)

FIGURE 5.45
(M = 20k)

FIGURE 5.46
(CL = 80cm)

Figures 5.43-5.46   Transmission electron micrographs of Nb-V
steel with austenitizing temperature
1250°C and finish rolling temperature
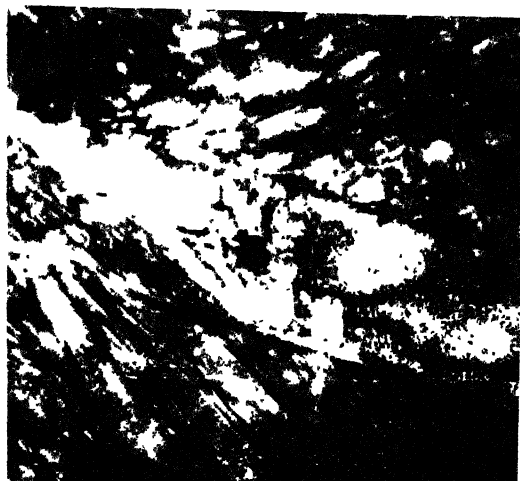1020°C, water quenched after 90% deforma-
tion (2RNQ).
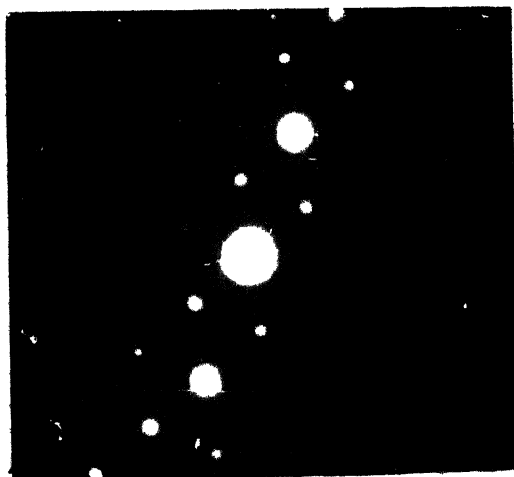
FIGURE 5.47
(M = 30k)

FIGURE 5.48
(M = 50k)

FIGURE 5.49
(M = 50k)

Figures 5.47-5.49   Transmission electron micrographs of Nb-V
steel with austenitizing temperature 1250°C
and finish rolling temperature 850°C, water
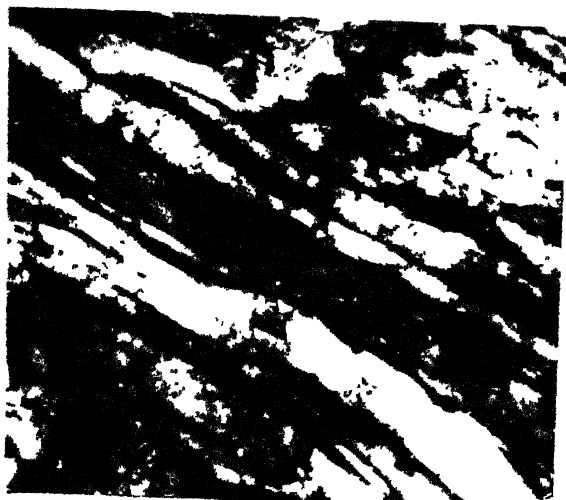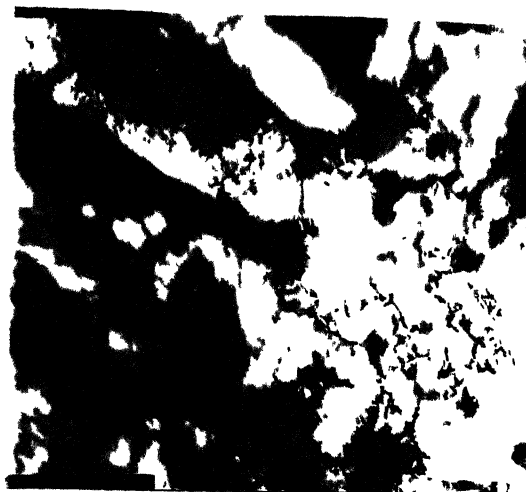quenched after 90% deformation (2NQ).

A correlation between the textures and microstructures of the controlled rolled steels can now be attempted at. The textures of the plain C steel finish rolled at 1020°C and 850°C are pretty similar and both are rather weak in intensity. The corresponding optical and electron microstructures are also quite similar, showing large equiaxed grains of ferrite. This indicates that the α grains, in both the cases, have been derived predominantly from recrystallized γ. Evidently finish rolling at 850°C has not changed the recrystallized character of the γ grains. The sharpness of the texture improves marginally after finish rolling at 730°C ($\alpha + \gamma$ range), although the nature of the texture remains very much similar, indicating that the texture at this stage is also dictated mostly by recrystallized γ grains transforming into ferrite. Some contribution may be made by the α grains formed from deformed γ. The contribution from any deformed ferrite (the volume percent of which is not expected to be much) seems to be minimal. This is quite in conformity with the optical microstructure which shows a much larger volume fraction of nearly equiaxed ferrite grains (obtained from recrystallized γ) and only a small volume fraction of ferrite obtained from unrecrystallized or partially recrystallized γ.

Although the texture of the Nb-V steel finish rolled at 1020°C is quite similar to the texture of the plain C steel with the same treatment, there is a remarkable change in the textures of the former with respect to the latter for lower finishing temperatures, such as 850°C and 730°C. The

textures of the Nb-V steel are found to be sharper as compared to their plain C counterparts. This is not unusual, since both optical and electron microstructures clearly indicate that the ferrite grains of the Nb-V steel at these stages must be derived predominantly from the unrecrystallized γ. Hence the intensities of the texture components such as {113} <110> and {332}<113> show perceptible sharpening in these cases.

After ferrite rolling (630°C), the texture will depend predominantly on the deformation behaviour of the ferrite which has inherited the textures of the recrystallized as well as the unrecrystallized γ. Since the rolling temperature here is pretty low, the effects of deformation of α will be very much retained and this will play a dominant role in the development of the α texture. The fact is that at this stage we should expect mainly a ferrite deformation texture, and this is not expected to be affected by factors other than the amount of rolling reduction. It is to be expected, therefore, that a rather similar crystallographic texture (of deformed ferrite) and microstructure (of deformed ferrite grains) should form in both the plain C and the Nb-V steel. This is precisely what has been obtained experimentally.

Chapter VI

Conclusions

1. The textures of the plain C steel, finish rolled at
    1020°C, 850°C and 730°C are not much different from one
    another. Each of them is rather weak and consist of the
    components {100}<011>, {113}<110> and {332}<113>. After
    ferrite rolling (at 630°C) the intensity of the texture
    components increase markedly.

2. For the Nb-V steel finish rolled at 1020°C the texture
    is quite similar to that of the corresponding plain C
    steel. Marked increase in the intensities is noticed
    for the components {113}<110> and {332}<113>, after
    finish rolling at 850°C and 730°C. The texture of the
    Nb-V steel after finish rolling at 630°C is practically
    similar to that of the corresponding plain C steel.

3. The optical microstructures of the plain C and the Nb-V
    steels are quite similar, after finish rolling at 1020°C,
    and show equiaxed ferrite grains derived basically from
    recrystallized γ. While similar microstructures are
    obtained for the plain C steel even after finish rolling
    at 850°C and 730°C, the corresponding microstructures in
    the Nb-V steel show that here the ferrite grains are
    derived basically by transformation from unrecrystallized
    γ. Finally, after finish rolling at 630°C, the

microstructures of both the plain C and the Nb-V steel show deformed ferrite grains only.

4. The grain size measurements show that the sizes of the ferrite grains are dependent on the austenitizing temperature, amount of rolling reduction and finishing temperature. Other factor remaining constant, finer ferrite grains are obtained for the Nb-V steel as compared to the plain C steel. In general, controlled rolling at progressively lower temperatures, starting from the γ recrystallization range and finishing in the ferrite range, produces the finest ferrite grain size.

5. The results of electron microscopic studies are in broad conformity with the optical microscopy results. The structural details, obtained by both optical and electron microscopy, have been found to correlate reasonably well with the macroscopic textural results for both the experimental steels. A sharp texture in any of the steels can be related to either ferrite obtained from unrecrystallized γ by transformation or ferrite which has been heavily deformed. On the other hand a weak ferrite texture corresponds to nearly equiaxed ferrite grains obtained predominantly by transformation from recrystallized γ.

References

1. W.J. Berry: Iron Coal Trade Rev., 66 (1928) 900.

2. H. Hanemann and F. Lucke: Stahl Eisen, 45 (1925) 1117-1122.

3. R.W. Vanderbeck: Weld J., 37 (1958) 1145-1165.

4. C.A. Beiser: Preprint 138, Annual Convention ASM, Chicago, 1959.

5. A. Arrowsmith: J. Iron Steel Inst., 110 (1924) 317-319.

6. W. Barr and C.F. Tipper: J. Iron Steel Inst., 157 (1947) 223-238.

7. I.M. Mackenzie: J. West Scotland Iron Steel Inst., 60 (1952-53) 224-258.

8. J.M. Hodge, R.D. Manning, and H.M. Reichhold: Trans. AIME, 185 (1949) 233-240.

9. R.H. Frazier, F.W. Boulger, and C.H. Lorig: Iron Steel Eng., 33 (Oct. 1956) 66-67.

10. E.O. Hall: Proc. Phys. Soc., 64B (1951) 747-753.

11. J. Heslop and N.J. Petch: Philos. Mag., 3 (1958) 1128-1136.

12. H.J. Wiester, W. Dahl, and H. Hengstenberg: Stahl Eisen, 82 (1962) 1176-1186.

13. M. Haneke: Arch. Eisenhuttenwes., 33 (1962) 233-239.

14. T.M. Noren: Ship Structure Committee Special Report, 1963, SSC-154.

15. W.E. Duckworth, R. Phillips, and J.A. Chapman: J. Iron Steel Inst., 203 (1965) 1108-1114.

16. R. Phillips and J.A. Chapman: J. Iron Steel Inst., 204 (1966) 615-622.

17. J.J. Irani, D. Burton, J.D. Jones, and A.B. Rothwell: Strong Tough Structural Steels, London, The Iron and Steel Institute, (1967) 110-122.

18. J.D. Jones and A.B. Rothwell: 'Deformation under Hot Working Conditions', London, The Iron and Steel Institute, (1968) 78-82.

19. S. Mishra and C. Darmann: Int. Met. Rev., 27(6) (1982) 307.

20. W.B. Hutchinson: Int. Met. Rev., 29(1) (1984) 25.

21. T. Tanaka: Int. Met. Rev., 26(4) (1981) 185.

22. H. Inagaki: in Proc. 6th Int. Conf. on 'Textures of Materials', Tokyo, The Iron and Steel Institute of Japan, 1 (1981) 149.

23. R.K. Ray and J.J. Jonas: Int. Mat. Rev., 35(1) (1990) 1.

24. I. Kozasu, T. Shimizu, and H. Kubota: Trans. Iron Steel Inst. of Japan, 11 (1971) 367-375.

25. H. Matsubara, T. Osuka, I. Kozasu, and K. Tsukada: Trans. Iron Steel Inst. of Japan, 12 (1972) 435-443.

26. J.D. Baird and R.R. Preston: 'Processing and properties of low-carbon steel', 1-46; 1973, New York, Metallurgical Society of AIME.

27. M. Fukuda, T. Hashimoto, and K. Kunishige: 'Microalloying '75', 120-135; 1977, New York, Union Carbide Corporation.

28. M. Fukuda, T. Hashimoto, and K. Kunishige: Tetso-to-Hagane, 58 (1972) 1832-1847.

29. H. Sekine and T. Maruyama: Seitetsu Kenkyu, 289 (1976) 11920-11937.

30. I. Kozasu, C. Ouchi, T. Sanpei, and T. Okita: Microalloying '75, New York, Union Carbide Corporation, (1977) 120-135.

31. T. Coleman, D. Dulieu, and A. Gouch: 'The microstructure and design of alloys', London, The Metals Society, 1 (1974) 70-74.

32. T. Gladman and D. Dulieu: Met. Sci., 8 (1974) 167-176.

33. T. Tanaka, N. Tabata, T. Hatomura, and C. Shiga: Microalloying '75, New York, Union Carbide Corporation, (1977) 107-119.

34. T. Tanaka, T. Hashimoto, and N. Tabata: Kawasaki Steel Tech. Rep., 6 (1974) 522-537.

35. W.J. McG. Tegart and A. Gittins: 'The hot deformation of austenite', New York, American Institute of Mining, Metallurgical and Petroleum Engineers, (1977) 1-67.

36. H.J. McQueen: J. Met., April 20 (1968) 31-38.

37. C. Ouchi, T. Okita, T. Sanpei, and I. Kozasu: Tetsu-to-Hagane, 63 (1977) A53-A56.

38. D.J. Towle and T. Gladman: Met. Sci., 13 (1979) 246-256.

39. C. Ouchi, T. Sanpei, T. Okita, and I. Kozasu: 'The hot deformation of austenite', New York, American Institute of Mining, Metallurgical and Petroleum Engineers (1977) 316-340.

40. T. Tanaka: 'Hot deformation of steels', Tokyo, The Iron and Steel Institute of Japan, (1980) 23-49.

41. T. Tanaka, T. Funakoshi, M. Ueda, T. Yasuda, J. Tsuboi, and C. Utahashi: 'Microalloying '75', New York, Union Carbide Corporation, (1977) 399-409.

42. T. Hatomura and T. Tanaka: Tetsu-to-Hagane, 62 (1976) S206.

43. T. Tanaka, T. Hatomura, and N. Tabata: Tetsu-to-Hagane, 62 (1976) S206.

44. A. Le Bon and L.N. de Saint-Martin: 'Microalloying '75', New York, Union Carbide Corporation, (1977) 90-99.

45. K.J. Irvine, T. Gladman, J. Orr, and F.B. Pickering: J. Iron Steel Institute, 208 (1970) 717-726.

46. I. Kozasu: Trans. Iron Steel Inst. Jpn., 12 (1972) 241-250.

47. A. Le Bon, J. Rofes-Vernin, and C. Rossard: Mem. Sci. Rev. Metall., 70 (1973) 577-588.

48. J.J. Jonas and I. Weiss: Met. Sci., 13 (1979) 238-245.

49. M. Lamberigts and T. Greday: 'The hot deformation of austenite', New York, American Institute of Mining, Metallurgical and Petroleum Engineers, (1977) 286-315.

50. R. Coladas, J. Masounave, and J.P. Bailon: 'The hot deformation of austenite', New York, American Institute of Mining, Metallurgical and Petroleum Engineers (1977) 341-383.

51. I. Weiss and J.J. Jonas: Metall. Trans. 10A (1979) 831-840.

52. H. Sekine and T. Maruyama: Trans. Iron Steel Inst. Jpn., 16 (1976) 427-436.

53. A.B. Rothwell: Mem. Sci. Rev. Metall., 69 (1972) 413-424.

54. R. Priestner: Rev. Metall., 72 (1975) 285-296.

55. A. Le Bon, J. Rofes-Verais, and C. Rossard: Met. Sci., 9 (1975) 36-40.

56. S. Sekino, N. Mori, and S. Tamukai: Tetsu-to-Hagane, 58 (1972) 1044-1053.

57. H. Watanabe, Y.E. Smith, and R.D. Pelke: 'The hot deformation of austenite', New York, American Society of Mining, Metallurgical and Petroleum Engineers, (1977) 140-168.

58. A.T. Davenport, R.E. Miner, and R.A. Kot: 'The hot deformation of austenite', New York, American Institute of Mining, Metallurgical and Petroleum Engineers, (1977) 186-203.

59. T.G. Oakwood, W.E. Heitman, and E.S. Madrzyk: 'The hot deformation of austenite', New York, American Institute of Mining, Metallurgical and Petroleum Engineers, (1977) 204-232.

60. K.J. Irvine and T.N. Baker: Met. Sci., 13 (1979) 228-237.

61. E.L. Brown, A.J. De Ardo, and J.H. Bucher: 'The hot deformation of austenite', New York, American Institute of Mining, Metallurgical and Petroleum Engineers, (1977) 250-285.

62. B.F. Decker, E.T. Asp, and D. Harker: J. Appl. Phys., 19 (1948) 388.

63. L.G. Schulz: J. Appl. Phys., 20 (1949) 1030.

64. H. Inagaki: Z. Metallkd., 75 (1984) 510.

65. H. Inagaki: Z. Metallkd., 79 (1988) 716.

66. F.H. Samuel, R. Barbosa, F. Boratto, S. Yue, and J.J. Jonas: in Proc. Int. Conf. on 'Physical Metallurgy of Thermomechanical Processing of Steels and Other Metals', Tokyo, The Iron and Steel Institute of Japan, 2 (1988) 721.

67. H. Hu and J.S. Kallend: in Proc. 6th Int. Conf. on 'Textures of Materials', Tokyo, The Iron and Steel Institute of Japan, 1 (1981) 164.

68. J.S. Kallend, P.P. Morris, and G.J. Davies: Acta Metall.

69. H. Inagaki: Z. Metallkd., 74 (1983) 716.

70. G.J. Davies: in Proc. 5th Int. Conf. on 'Texture of Materials', Berlin, Springer-Verlag, 2 (1978) 121.

71. T. Nakamura, T. Sakaki, Y. Roe, E. Fukushima, and H. Inagaki: Trans. Iron Steel Inst. Jpn., 15 (1975) 561.

72. H. Inagaki: Trans. Iron Steel Inst. Jpn., 17 (1977) 166.

73. H. Inagaki: in Proc. 5th Int. Conf. on 'Texture of Materials', Berlin, Springer-Verlag, 2 (1978) 157.

74. G.J. Davies and R.M. Bateman: in Proc. 6th Int. Conf. on 'Texture of Materials', Tokyo, The Iron and Steel Institute of Japan, 1 (1981) 132.

75. J.H. Little, J.A. Chapman, W.R. Morrison, and B. Mintz: in 'The microstructure and design of alloys', London, The Metals Society, 1 (1974) 80.

76. T. Tanaka and N. Tabata: Tetsu-to-Hagane (J. Iron Steel Inst. Jpn.), 64 (1978) 1353.

77. H. Inagaki and M. Kodama: Tetsu-to-Hagane (J. Iron Steel Inst. Jpn.), 67 (1981) 5640.

78. L.S. Toth, R.K. Ray, and J.J. Jonas: Metall. Trans. A, (1990) 2985-3000.

79. H. Inagaki, K. Kunihara, and I. Kozasu: Trans. Iron Steel Inst. Jpn., 17 (1977) 75.

80. G.F. Melloy and J.D. Dennison: in 'The microstructure and design of alloys', London, The Metals Society, 1 (1974) 60.

81. H. Saitoh, K. Ushioda, T. Senuma, T. Nakamura, and K. Esaka: in Proc. Int. Conf. on 'Physical metallurgy of thermomechanical processing of steels and other metals', Tokyo, The Iron and Steel Institute of Japan, 2 (1988) 628.

82. T. Senuma and H. Yada: in Proc. Int. Conf. on 'Physical metallurgy of thermomechanical processing of steels and other metals', Tokyo, The Iron and Steel Institute of Japan.

83. T. Nakamura and K. Esaka: in Proc. Int. Conf. on 'Physical metallurgy of thermomechanical processing of steels and other metals', Tokyo, The Iron and Steel Institute of Japan, 2 (1988) 644.

84. S. Hashimoto, T. Yakashiji, T. Kashima, and K. Hosomi: in Proc. Int. Conf. on 'Physical metallurgy of thermo-mechanical processing of steels and other metals', Tokyo, The Iron and Steel Institute of Japan, 2 (1988) 652.

85. S. Hashimoto, T. Yakushiji, T. Kashima, and K. Hoshomi: in Proc. 8th Int. Conf. on 'Textures of materials', Warrendale, PA, The Metallurgical Society of AIME, (1988), 673.

86. L.N. Pussegoda, S. Yue, and J.J. Jonas, Metall: Trans., 21A (1990) 153-164.

87. C. Lang, W. Kapellner, R. Kaspar, and L. Meyer: Steel Res., 58 (1987) 465-471.

88. F. Boratto, S. Yue, J.J. Jonas, and T.H. Lawrence: Thermec-88, I. Tamura (ed.), The Iron and Steel Institute of Japan, 2 (1988) 519-526.

89. T. Senuma and H. Yada: in Annealing Processess - Recovery, Recrystallization and Grain Growth, N. Hansen et al. (eds.), Riso National Laboratory, Denmark (1986) 547-552.

90. C.M. Sellars: in Hot Working and Forming Processes, C.M. Sellers and G.J. Davies (eds.), The Metal Society, (1979) 3-15.

91. P. Coquet, A. Le Bon, and Ch. Perdrix: Proc. ICSMA-7, 2 (1985) 1031-1036.

92. J.H. Beynon, A.R.S. Ponter, and C.M. Sellars: 'Metallographic Verification of Computer Modelling of Hot Rolling' from 'Modelling of Metal Forming Processes', Eds. J.L. Chenot and E. Onate, Kluwer Academic Publishers, (1988) 321-328.

93. T. Senuma and H. Yada: Proc. 7th Riso Int. Symp. on Metallurgy and Materials Science, Riso, Denmark, (1986).

94. M. Suehiro, T. Senuma, H. Yada, Y. Matsumura, and T. Ariyoshi: Tetsu-to-Hagane, 73 (1987) 1026.

95. M. Suehiro, K. Sato, Y. Tsukano, H. Yada, T. Senuma, and Y. Matsumura: Trans. ISIJ, 27 (1987) 439.

96. M. Suehiro, K. Sato, Y. Tsukano, H. Yada, T. Senuma, H. Shigefuji, and Y. Yamashita, Thermec-88, 2 (1988) 791.

97. H. Yada: Proc. Int. Symp. Accelerated Cooling of Rolled Steel, The Metall. Soc. CIM, Montreal, Winnipeg, Canada, (1987) 105.

98. J.C. Cabanas-Moreno, L.C. Alcibar-Pena, I. Hernandez-Dimayuga, G. Hernandez-Uribe, and J.J. Cruz-Rivera: in Proc. of the Int. Symp. on 'Mathematical modelling of hot rolling of steel', (Ed.) S. Yue, Hamilton, Ontario, Canada, (1990) 119-127.

99. J.H. Beynon, P.R. Brown, S.I. Mizban, A.R.S. Ponter, and C.M. Sellars: 'Inclusion of Metallurgical Development in the Modelling of Industrial Hot Rolling of Metals' from 'Nuniform '86', (Eds.) K. Mattiasson et al. and A.A. Balkema, (1986) 213-218.

100. J.H. Beynon, P.R. Brown, S.I. Mizban, A.R.S. Ponter, and C.M. Sellars: 'An Eulerian Finite Element Method for the Thermal and Viscoplastic Deformation of Metals in Industrial Hot Rolling', from 'Computational Methods for Predicting Material Processing Defects', (Ed.) M. Predeleanu, Elsevier, (1987) 19-28.

101. R.A. Harding: Ph.D. thesis, University of Sheffield, 1976.

102. C.M. Sellars and J.A. Whiteman: Metal Science, 13 (1979) 187-194.

103. C.M. Sellars: Materials Science and Technology, 1 (1985) 325-332.

104. R.A.N.M. Barbosa, Ph.D. thesis, University of Sheffield, 1983.

105. S. Gorman: Final year project report, University of Sheffield, 1989.

106. A. McLaren, J.H. Beynon, and C.M. Sellars: in Proc. of the Int. Symp. on Mathematical Modelling of Hot Rolling of Steel (Ed.), S. Yue, Hamilton, Ontario, Canada, (1990) 138-147.

107. M. Suehiro, H. Yada, T. Senuma, and K. Sato: in Proc. of the Int. Symp. on Mathematical Modelling of Hot Rolling of Steel (Ed.), S. Yue, Hamilton, Ontario, Canada, (1990) 128-137.

108. K.J. Irvine and F.B. Pickering: JISI, 187 (1957) 292.

109. S. Akamatsu, T. Senuma, and H. Yada: in Proc. of the Int. Symp. on Mathematical Modelling of Hot Rolling of Steel (Ed.), S. Yue, Hamilton, Ontario, Canada, (1990) 467-476.

110. M. Fujioka, A. Yoshie, H. Morikawa, and M. Suehiro: Camp-ISIJ, 2 (1989) 692.

111. H. Yada: in 'Accelerated Cooling of Rolled Steel',
      G.E. Ruddle and A.F. Crawley (eds.), Pergamon Press,
      1988.

112. T. Senuma, H. Yada, Y. Matsumara and T. Futamara: Tetsu-
      to Hagane, 70 (1984) 2112-2119.

113. B.D. Cullity: 'Elements of X-ray Diffraction', 2nd ed.,
      Addison-Wesley Pub. Co. Inc., (1978) 308.

ME-1991-M-BHA-TEX